STUDY OF TANDEM HELICOPTER ROTOR-ROTOR INTERFERENCE EFFECTS ON THE THRUST OF THE REAR ROTOR

by

ANADI S. SARKAR

B.M.E., College of Engineering and Technology
Jadavpur (INDIA)
(1950)

SUBMITTED IN PARTIAL FULFILLMENT
OF THE REQUIREMENTS FOR THE
DEGREE OF MASTER OF SCIENCE

at the

MASSACHUSETTS INSTITUTE OF TECHNOLOGY

August, 1963

Signature of Author Signature redacted
Department of Aeronautics
and Astronautics, August 1963

Certified by Signature redacted
Thesis Supervisor

Accepted by Signature redacted
Chairman, Departmental
Graduate Committee

STUDY OF TANDEM HELICOPTER ROTOR-ROTOR INTERFERENCE EFFECTS ON THE THRUST OF THE REAR ROTOR

by

Anadi S. Sarkar

Submitted to the Department of Aeronautics and Astronautics on August 19, 1963 in partial fulfillment of the requirement for the degree of Master of Science.

ABSTRACT

The induced velocity of a single rotor helicopter can be calculated by the momentum theory. But the momentum theory can not determine the induced velocity at the rear rotor of a tandem helicopter in forward flight. The total inflow of the rear rotor of a tandem helicopter comprises the inflow caused by the rear rotor itself and the interference due to the front rotor. The interference effect was calculated from the contours of the induced velocity ratio of the front rotor at some distance, depending on the rotor overlap and stagger, behind it. By application of the above procedure at five different forward speeds and three overlap conditions, it was found that the thrust of the rear rotor varies directly with the forward speed and inversely with overlap, assuming that the other parameters of the rotors remain the same. The results were then compared with the experimental data. It was also found that the third harmonic is the predominant harmonic airload in all the cases.

It is recommended that the investigation be extended to rotors of various configurations, etc.; and through careful examination of the results it is likely that the induced velocity at the rear rotors can be expressed by an empirical equation.

Thesis Supervisor: Norman D. Ham

Title: Assistant Professor of Aeronautical Engineering

ACKNOWLEDGEMENT

The author is grateful to Professor Norman D. Ham for the counsel and criticism provided in the course of this investigation. The debt extended further to include the excellent teaching that made it possible for the author even to attempt an investigation in this field.

To Professor Rene H. Miller, author expresses his gratitude for the personal and professional inspiration received. Appreciation is expressed to Mr. Bob Cummings for his valuable assistance in the experimental work done, Mrs. Nancy Ghareeb of the M.I.T. Aeroelastic Laboratory Computing Section for her careful programming of solutions for harmonic analysis, and Mrs. Barbara Marks who sacrificed her week-ends to type the manuscript, and finally, to my wife, Anima, for her patience in enduring a year's separation.

TABLE OF CONTENTS

LIST OF FIGURES AND TABLES

Figures

Figures (Cont'd.)

Tables

Tables (Cont'd.)

LIST OF SYMBOLS

A_n = Cosine coefficient of nth harmonic in Fourier series

a = Aerofoil section lift-curve slope, radians

B_n = Sine coefficient of nth harmonic in Fourier series

b = Number of blades per rotor

C_T = Rotor thrust coefficient

c = Chord of the blade

g = Out of plane harmonic blade displacement

h/R = Rotor stagger

i = Rotor disc incidence, (^{o})

$\overline{K}$ = Mean steady-state value of the induced velocity ratio

l/R = Rotor overlap

m = Blade running mass, slugs/ft

N = Rotor speed, rpm

n = Harmonic order

R = Rotor radius, ft

r = Radial distance to blade element

S = Vertical shear, lb

T = Rotor thrust, lb

U = Induced velocity, ft/sec

U_T = Component at blade element of resultant velocity perpendicular to blade span axis and to axis of no feathering, ft/sec

U_P = Component at blade element of resultant velocity perpendicular to blade span axis and U_T, ft/sec

V = Forward velocity, ft/sec

X = Angle between axis of wake and axis of tip-path plane - wake angle

x = Ratio of blade element radius to rotor blade radius (r/R)

Z = Out of plane blade displacement

α = Angle of tilt of rotor shaft, ($^\circ$)

β = Flapping angle, ($^\circ$)

γ = Blade flapping Lock Number

η = Blade mode shape

θ = Collective pitch angle of the blades, ($^\circ$)

λ = Inflow ratio

λ' = Total inflow ratio

μ = Advance ratio

ρ = Mass density of air, slugs/cu ft

σ = Rotor solidity

ψ = Reference blade azimuth angle measured from downward position in the direction of rotation, ($^\circ$)

Ω = Rotor angular velocity, rad/sec

Subscripts and Superscripts

. = Differentiation with respect to time

c = Cosine component

s = Sine component

n = Harmonic order

h = Values taken with respect to the hub plane

t = Values taken with respect to the tip-path plane

F = Values taken with respect to the front rotor

R = Values taken with respect to the rear rotor

CHAPTER 1

INTRODUCTION

There are many instances in helicopter design where much can be gained from a knowledge of the correct induced velocity or inflow distribution throughout the rotor disc. Solutions of the problems of excessive vibration, structural fatigue, roughness of control and rotor interference would become more evident if the nature of the rotor disturbances were known. A better understanding of the vibratory loads would permit the design of rotor blades for minimum vibration by analytical means.

Several theoretical investigations have dealt with the problem of the induced velocities near a lifting rotor. Mangler and Squire, in Ref. 3, had computed the induced velocities in the rotor disc and in the transverse plane in the far wake. Reference 6 also gives the induced velocities throughout the longitudinal and lateral planes of a uniformly loaded rotor. Experimental results from a comprehensive rotor downwash investigation are presented in Ref. 4. Reference 1 presents an extensive compilation

of charts of the induced velocities near a lifting rotor for both uniform and nonuniform disc load distributions.

It can be shown that the results of Ref. 3, when modified, will correspond with the result of Ref. 1. The incidence i, used by Mangler, is the complement of the wake angle X of Heyson in Ref. 1. Induced velocity ratio, w/VC_T, of Mangler can be converted into $v/v_o \cdot 1/4 \tan X$ of Heyson.

The contours of induced velocity ratio for a wake angle of 76° at $\psi = 90^\circ$ and 270° have been plotted in Fig. 6, from both Heyson and Mangler's theory and they agree reasonably well.

In case of a single rotor helicopter, the steady state induced velocity can be calculated with the help of momentum theory. But, in case of a tandem helicopter, the total inflow of the rear rotor is influenced by the interference of the front rotor and as such the momentum theory can not be applied directly to determine the induced velocity. The charts of Ref. 1 can be made applicable to tandem helicopter and the induced velocity or total inflow distribution over the rotor discs of a tandem helicopter in forward flight can be found. Duvivier, in Ref. 2, has some experimental results which are useful in this study.

In a tandem rotor helicopter, the rear rotor is in a stream, which is inclined downwards due to the downwash

from the front rotor and this would cause a reduction in thrust, if it were not counterbalanced by a change in pitch of the blades or a change in inclination of the rotor axis.

The purpose of this paper is to determine the interference effect of the front rotor on the thrust of the rear rotor of a tandem helicopter in forward flight theoretically and compare the results with the experimental data. Theoretical and a partial experimental study of the harmonic vibratory forces at the rear rotor due to the front rotor was also made. As the present study is confined to three-bladed rotors, and since only the harmonics which are integers of the number of rotor blades appear as vibratory vertical shear at the rotor hub, only the third harmonic has been considered.

Table 1 lists the principal parameters of the rotors.

CHAPTER 2

THEORETICAL ANALYSIS

2.1 Determination of Front Rotor Wake Angle

Heyson, in Ref. 1, has presented the induced velocity charts for several nonuniform disc loadings and for a number of wake angles. The charts of this reference have been the basis of theoretical analysis of this paper. The hub plane has been taken as the reference plane, whereas the tip-path plane is the reference plane in Ref. 1. Hence, the inflow ratio with respect to tip-path plane has been used in Equation (6), to calculate the wake angle.

It has been assumed in this paper, as in Ref. 1, that the rotor wake vortex distribution consists of a straight elliptical cylinder formed by an uniform distribution of an infinite number of vortex rings of infinitesimal strength, lying in planes parallel to the tip-path plane and extending downstream to infinity. The wake angle is taken at the rotor, in the present analysis.

$$\lambda_{F_h} = \mu\alpha_F + \frac{C_T}{2\sqrt{\mu^2 + \lambda_{F_h}^2}} \quad , \quad \text{for} \quad \mu < .10 \qquad (1)$$

$$\approx \mu\alpha_F + \frac{C_T}{2\mu} \quad , \quad \text{for} \quad \mu \gg .10 \qquad (1a)$$

$$C_T = \frac{\sigma a}{2}\left[\frac{\theta_F}{3} - \frac{\lambda_{F_h}}{2}\right] \qquad (2)$$

From Equations (1a) and (2),

$$\lambda_{F_h} = \frac{\mu\alpha_F + \frac{\sigma a \theta_F}{12\mu}}{1 + \frac{\sigma a}{8\mu}} \qquad (3)$$

But,

$$\lambda_{F_t} = \lambda_{F_h} + \mu\beta_{1c} \qquad (4)$$

where,

$$\beta_{1c} = -\frac{\frac{8}{3}\left[\theta_F - \frac{3}{4}\lambda_{F_h}\right]\mu}{1 - \frac{1}{2}\mu^2} \qquad (5)$$

From Fig. (3),

$$\text{wake angle,} \quad \chi = \tan^{-1}\frac{\mu}{\lambda_{F_t}} \qquad (6)$$

2.2 Determination of Induced Velocity Ratio, U_{R_F}/U_F

In a tandem helicopter, the position of the rear rotor can be determined if the rotor overlap and stagger

is known. Reference 1 gives the contours of the induced velocity ratio in the longitudinal and lateral plane for different wake angles and disc loadings. From these contours, the ratio of induced velocity at the rear rotor due to the front rotor to the induced velocity of the front rotor, U_{R_F}/U_F, can be plotted against x_F/R for any wake angle and disc loading. The limits of x_F/R are determined by the rotor overlap.

Rotor Overlap	Limits of x_F/R in terms of Ref. 1
0	X/R to 3.00 X/R
.25	.75 X/R to 2.75 X/R
.50	.50 X/R to 2.50 X/R

The induced velocity ratio, U_{R_F}/U_F, in the lateral plane of the rotor is plotted against the blade station, maintaining the same trend of the induced velocity contours of Ref. 1.

From the graphs of induced velocity ratio, U_{R_F}/U_F, in both longitudinal and lateral plane, Figs. 7-12, the value of U_{R_F}/U_F is approximated by Fourier series as,

$$\frac{U_{R_F}}{U_F} = K(x) + \sum_{n=0}^{\infty} \left[A_n(x) \cos n\psi + B_n(x) \sin n\psi \right] \qquad (7)$$

$$\left[\frac{U_{R_F}}{U_F}\right]_{mean} = \frac{1}{2\pi R}\int_0^{2\pi}\int_0^{R}\frac{U_{R_F}}{U_F}\,dr\,d\psi \tag{8}$$

$$= \bar{K} \tag{8a}$$

2.3 Determination of Total Inflow Distribution of the Rear Rotor

The total inflow of the rear rotor comprises of inflow caused by the rear rotor as well as that due to the interference of the front rotor, and is given by

$$\lambda_R' = \lambda_R + \bar{K}\cdot\frac{U_F}{\Omega R} \tag{9}$$

But,

$$\lambda_R = \mu\alpha_R + \frac{C_{T_R}}{2\mu}\,, \quad \text{for } \mu \geq .10$$

$$= \mu\alpha_R + \frac{\bar{\sigma}a}{4\mu}\left[\frac{\theta_R}{3} - \frac{\lambda_R'}{2}\right] \tag{10}$$

And,

$$\frac{U_F}{\Omega R} = \frac{C_{T_R}}{2\mu}\,, \qquad \text{for } \mu \geq .10$$

$$= \frac{\bar{\sigma}a}{4\mu}\left[\frac{\theta_F}{3} - \frac{\lambda_{F_n}}{2}\right] \tag{11}$$

From Equations (9), (10) and (11), for $\mu \geq .10$,

$$\lambda_R' = \frac{\mu a_R + \frac{\sigma a \theta_R}{12\mu} + \left[\frac{\sigma a}{4\mu}\left(\frac{\theta_F}{3} - \frac{\lambda_{Fn}}{2}\right)\right]\bar{K}}{1 + \frac{\sigma a}{8\mu}} \qquad (12)$$

2.4 Determination of the Thrust of the Rear Rotor with Interference Effect

The thrust of the rear rotor can be calculated either using the mean value of U_{R_F}/U_F as given in Equation (8) or by using the complete Fourier series representation of U_{R_F}/U_F, Equation (7).

From Equation (8-15) of Ref. 5, the differential thrust of the rear rotor,

$$dT_R = \tfrac{1}{2}\rho a\left[\theta_R U_T^2 - U_P U_T\right] c.dr \qquad (13)$$

$$U_T = \Omega r + \mu \Omega R \sin\psi \qquad (14)$$

$$U_P = \lambda_R' \Omega R + r\dot{\beta} + \mu \Omega R \beta \cos\psi \qquad (15)$$

The total thrust produced by a rotor of b blades is found by integrating the differential thrust, Equation (13), around the azimuth and then along the blade span, and is given by

$$T_R = \frac{1}{4\pi}\rho a b c \int_0^{2\pi}\int_0^R \left[\theta_R U_T^2 - U_P U_T\right] dr\, d\psi \qquad (16)$$

Inserting Equation (14) and (15) in equation (16),

$$T_R = \tfrac{1}{2}\rho a b c \Omega^2 R^3 \left[\frac{\theta_R}{3}\left(1+\frac{3}{2}\mu^2\right) - \frac{\lambda_R'}{2} \right] \qquad (17)$$

The two methods of calculating the thrust of the rear rotor are explained below:

(a) From the average value of U_{R_F}/U_F

Using the average or mean value of U_{R_F}/U_F, in Equation (12), the average value of λ_R' was calculated, which was then substituted in Equation (17) to obtain the thrust of the rear rotor.

(b) From the Fourier series representation of U_{R_F}/U_F

Equation (7), which gives the Fourier series representation of U_{R_F}/U_F, is inserted into Equation (12) to obtain a more accurate value of λ_R'. Equation (12) then reduces to

$$\lambda_R' = \frac{\mu d_R + \frac{\sigma a \theta_R}{12\mu} + \left[\frac{\sigma a}{4\mu}\left(\frac{\theta_F}{3} - \frac{\lambda_{F_n}}{2}\right)\right]\left[K + \sum_{n=0}^{\infty}\left(A_n \cos n\psi + B_n \sin n\psi\right)\right]}{1+\frac{\sigma a}{8\mu}} \qquad (18)$$

Inserting Equation (18) into Equation (15), and then using Equation (14), (15) and (16),

$$T_R = \frac{1}{4\pi}\rho abc \int_0^{2\pi}\int_0^{R} \left[\theta_R(\Omega r + \mu\Omega R \sin\psi)^2 - (\Omega r + \mu\Omega R \sin\psi)\right.$$

$$\left\{\frac{\mu\alpha_R + \frac{\sigma a \theta_R}{12\mu} + \frac{\sigma a}{4\mu}\left(\frac{\theta_F}{3} - \frac{\lambda_{Fh}}{2}\right)\left[K + \sum_{n=0}^{\infty}\left(A_n \cos n\psi + B_n \sin n\psi\right)\right]}{1 + \frac{\sigma a}{8\mu}}\right\}$$

$$\left.\Omega R + r\dot{\beta} + \mu\Omega R\beta\cos\psi\right] dr\, d\psi \qquad (19)$$

Later work shows that the harmonic inflow is predominantly of third order and other harmonics are insignificant. As the third harmonic does not affect the steady-state thrust, the thrust given by Equations (17) and (19) will not differ much.

2.5 Determination of the Thrust of the Rear Rotor Without Interference Effect

When there is no interference, the inflow is given by

$$\lambda_R = \mu\alpha_R + \frac{C_T}{2\sqrt{\mu^2 + \lambda_R^2}}, \quad \text{for } \mu < .10 \qquad (20)$$

$$\approx \mu\alpha_R + \frac{C_T}{2\mu}, \quad \text{for } \mu \geq .10 \qquad (20a)$$

$$C_T = \frac{\sigma a}{2}\left[\frac{\theta_R}{3} - \frac{\lambda_R}{2}\right] \tag{21}$$

From Equations (20a) and (21), for $\mu \geq .10$,

$$\lambda_R = \frac{\mu \alpha_R + \frac{\sigma a \theta_R}{12\mu}}{1 + \frac{\sigma a}{8\mu}} \tag{22}$$

and inserting the value of λ_R, obtained from Equation (22) in Equation (17), in place of λ_R',

$$T_R = \tfrac{1}{2}\rho a b c \Omega^2 R^3\left[\frac{\theta_R}{3}\left(1 + \frac{3}{2}\mu^2\right) - \frac{\lambda_R}{2}\right] \tag{23}$$

2.6 Harmonic Loads

For harmonic analysis, the induced velocity ratio of any station at least at twelve different points around the azimuth is essential. In section 2.2, the method of determining the induced velocity ratio in the longitudinal and the lateral plane has been explained. For harmonic analysis, the induced velocity ratios for $\psi = 45^\circ$, 135°, 225° and 315° were also determined.

The induced velocity ratio against the azimuth for $x = .25$, $.50$, $.75$ and 1.0 for the following cases were drawn, Figs. 16-23:

(a) $\mu = .05$, $l/R = 0$, $h/R = .25$;

(b) $\mu = .05$, $l/R = .25$, $h/R = .25$;

(c) $\mu = .05$, $l/R = .50$, $h/R = .25$;

(d) $\mu = .10$, $l/R = .25$, $h/R = .25$.

From the figures mentioned above, it is seen that the third harmonic is predominant. Hence, the cosine and the sine components of the third harmonic vibratory forces were calculated as explained hereafter.

The values of induced velocity ratio at an interval of 30° was obtained from these figures, and they were introduced into a program set up on the MIT G.P LGP 30 computer and $U_{R_{F_C}}/U_F$ and $U_{R_{F_S}}/U_F$ up to the fourth harmonic at various spanwise stations (x = .25, .50, .75 and 1.0) were obtained.

Following Ref. 7, the expression for the blade displacement was taken as

$$Z_n = r\beta_n + \eta g_n \tag{23a}$$

where the first flexible mode shape

$$\eta = 4\frac{r^2}{R} - 3r \tag{23b}$$

and the modal displacement equations with n = 3, neglecting second and fourth harmonic inflow coefficient are

$$\beta_{3_c} = \frac{\gamma}{16}\left[\int_0^1 x^2 \lambda_{3_c}\, dx + \frac{3}{4}\beta_{3_s} + \frac{3}{20} g_{3_s}\right] \tag{24}$$

$$\beta_{3_s} = \frac{\gamma}{16}\left[-\frac{3}{4}\beta_{3_c} - \frac{3}{20} g_{3_c}\right] \tag{25}$$

$$\int_0^1 x \frac{\eta}{R} \lambda_{3_c}\, dx + \frac{3}{20}\beta_{3_s} + \frac{21}{60} g_{3_s} = 0 \tag{26}$$

$$\frac{3}{20}\beta_{3_c} = -\frac{21}{60} g_{3_c} \tag{27}$$

By solving Equations (24), (25), (26) and (27) simultaneously, the modal displacements were obtained and introduced into the equations for the third harmonic vertical hub shears:

$$S_{3_c} = m\Omega^2 R^2\left[-\frac{\gamma}{6}\int_0^1 x \lambda_{3_c}\, dx - \frac{\gamma}{6}\beta_{3_s} + \frac{9}{2}\beta_{3_c} - \frac{3}{2} g_{3_c}\right] \tag{28}$$

$$S_{3_s} = m\Omega^2 R^2\left[\frac{\gamma}{6}\beta_{3_c} + \frac{9}{2}\beta_{3_s} - \frac{3}{2} g_{3_s}\right] \tag{29}$$

λ_{3_c} was calculated from the computer result, Table 10, and the values of the expressions $\int_0^1 x \lambda_{3_c}\, dx$, $\int_0^1 x^2 \lambda_{3_c}\, dx$

and $\int_0^1 x \frac{\eta}{R} \Gamma_{3c}\, dx$ were calculated by graphical integration.

The vibratory loads due to interference effects are tabulated in Table 11. The sample calculation with zero overlap, quarter radius stagger and at $\mu = .05$ is shown in section 2.8.

2.7 Parametric Study

Theoretical analyses were carried out for the following rotor parameters, besides those given in Table 1.

Angle of tilt of the rotor shaft:		Front rotor = 10° Rear rotor = 5°
Collective pitch angle of the blades:		Front rotor = 10° Rear rotor = 10°
Rotor overlap,	l/R	0, .25, .50
Rotor stagger,	h/R	.25
Rotor speed,	N	400 rpm
Advance ratio,	μ	.05, .10, .15, .20, .25
Disc loading,		Typical and Uniform

The results of the analysis are placed at Tables 2-7. Table 9 gives the rear rotor thrust without interference.

The sample calculation is shown in section 2.8.

2.8 Sample Calculation

(a) Thrust of the rear rotor with interference effect:

$l/R = .25$ $\quad h/R = .25$ $\quad \mu = .10$

Disc loading . . . . . Typical

From equation (3),

$$\tau_{F_h} = \frac{(.10 \times .174) + \frac{.0995 \times 5.67 \times .174}{12 \times .10}}{1 + \frac{.0995 \times 5.67}{8 \times .10}}$$

$$= .058$$

From equation (5),

$$\beta_{1c} = -\frac{\frac{8}{3} \times .10 \left[.174 - \frac{3}{4} \times .058 \right]}{1 - \frac{1}{2}(.10)^2}$$

$$= -.035$$

From equation (4)

$$\tau_{F_t} = .058 + (.10 \times -.035)$$

$$= .0545$$

From equation (6)

$$\chi = \tan^{-1} \frac{.10}{.0545}$$

$$= 61.5^\circ$$

From Fig. 7

$$\bar{K} = .60$$

From equation (12)

$$\lambda'_R = \frac{(.10 \times .087) + \frac{.0995 \times 5.67 \times .174}{12 \times .10} + \frac{.0995 \times 5.67}{4 \times .10}\left(\frac{.174}{3} - \frac{.058}{2}\right).60}{1 + \frac{.0995 \times 5.67}{8 \times .10}}$$

$$= .0676$$

From equation (17)

$$T_R = \frac{1}{2} \times .002378 \times 5.67 \times 3 \times \frac{5}{12} \times (167.5)^2 \times 4\left[\frac{.174}{3}\left(1 + \frac{3}{2} \times .10^2\right) - \frac{.0676}{2}\right]$$

$$= 23.9 \text{ lbs.}$$

(b) Thrust of the Rear Rotor Without Interference:

$$\alpha_R = 5^\circ \text{ or } .087 \text{ rad.}$$

$$\theta_R = 10^\circ \text{ or } .174 \text{ rad.}$$

$$\mu = .10$$

From equation (22)

$$\lambda_R = \frac{(.10 \times .087) + \frac{.0995 \times 5.67 \times .174}{12 \times .10}}{1 + \frac{.0995 \times 5.67}{8 \times .10}}$$

$$= .053$$

From equation (23)

$$T_R = \frac{1}{2} \times .002378 \times 5.67 \times 3 \times \frac{5}{12} \times (167.5)^2 \times 4\left[\frac{.174}{3}\left(1 + \frac{3}{2} \times .10^2\right) - \frac{.053}{2}\right]$$

$$= 30.8 \text{ lbs.}$$

(c) Third harmonic Vertical Shears:

$$\frac{U_F}{\Omega R} = \frac{.0995 \times 5.67}{4 \times .05}\left[\frac{.174}{3} - \frac{.068}{2}\right]$$

$$= .04$$

From the computer result $\frac{U_{R_{F_{3c}}}}{U_F}$,

$= -.053$ at $x = .25$

$= -.078$ at $x = .50$

$= -.18$ at $x = .75$

$= -.26$ at $x = 1.0$

$$\Gamma_{3c} = \frac{U_{R_{F_{3c}}}}{U_F} \times \frac{U_F}{\Omega R}$$

$\therefore$ Γ_{3c} at various spanwise station:

x	Γ_{3c}
.25	-.00212
.50	-.00312
.75	-.0072
1.0	-.0104

By graphical Integration,

$$\int_0^1 x \Gamma_{3c}\, dx = -.00317$$

$$\int_0^1 x^2 \Gamma_{3c}\, dx = -.0025$$

$$\int_0^1 x \frac{\eta}{R} \Gamma_{3c}\, dx = -.001$$

Applying equations (24) to (27),

$$\beta_{3c} = -.000525$$

$$\beta_{3s} = .0000945$$

$$g_{3c} = .000225$$

$$g_{3s} = .00281$$

Substituting the values in equations (28) and (29)

$$S_{3c} = .015 \times (167.5)^2 \left\{ \frac{4.2}{6} \times .00317 - \frac{4.2}{6} \times .0000945 - \frac{9}{2} \times .000525 - \frac{3}{2} \times .000225 \right\}$$

$$= -.23 \text{ lbs}$$

$$S_{3s} = .015 \times (167.5)^2 \left\{ -\frac{4.2}{6} \times .000525 + \frac{9}{2} \times .0000945 - \frac{3}{2} \times .00281 \right\}$$

$$= -1.74 \text{ lbs}$$

CHAPTER 3

3.1 Model and the Test Equipment

For the experimental program, the model and the test equipment described in Ref. 2 were used.

Briefly, both the rotors are eight feet in diameter, three bladed, fully articulated rotors with no cyclic pitch and mounted on pylons. The pylons are mounted on heavy steel beams in such a way that the front pylon can be moved fore and aft to vary the rotor overlap. Both the front and rear pylons can be raised by increments of six inches (R/8) in order to vary the rotor stagger. The pylons also have the provision to tilt the rotor heads from 0° to 20° forward. The power is supplied by a Vickers hydraulic motor, controlled from outside the tunnel. Two gear boxes and an intermediate shaft with Con Vel constant velocity joints operate the front rotor shaft synchronously with the rear shaft, in the opposite direction.

To operate as a single rotor configuration, the front rotor along with its pylon was removed. The single and the tandem rotor set up is shown in Figs. 4 and 5.

The shears were measured by means of a four arm strain gauge bridge reading the bending moment deflections of the springs when a vertical load was applied at the hub.

Thirty-three slip rings are used to transmit load and pressure signals from the rotating hub to the amplfiers and recording equipment. A timing mark is recorded every time the instrumented blade passes through the azimuth $\psi = 90^{\circ}$. The readings from the shears were linear over the whole range of measurements.

The rotor rpm was monitored by means of a Strobotac and at the desired rpm the shear channel was switched on and the shear values were recorded on the oscillograph.

3.2 Wind Tunnel

All the tests were conducted in the 9' x 11 1/2' return section of the Aeroelastic and Structures Research Laboratory Flutter Tunnel at M.I.T.

No corrections were applied to the data to account for the effects of tunnel wall interference. Although such corrections would effect the magnitude of the resultant downwash, it is expected that they would not significantly influence the overall conclusions that are drawn from the results.

3.3 Test Procedure

Tests were run on straight blades with the parameters mentioned in section 2.7. The experimental as well as the theoretical results are given in Table 8.

An attempt was also made to investigate the harmonic vibratory loads at the rear rotor due to the front rotor only. The pitch of the rear rotor blades were set at 0° for this purpose, the parameters were:

$\alpha_R = 5^\circ$ $\quad \theta_R = 0^\circ$ $\quad \alpha_F = 10^\circ$ $\quad \theta_F = 10^\circ$

$l/R = 0$ and $.25$

$h/R = .25$

$\mu = .05, \quad .10 \quad .15$

$N = 400$ rpm

Table 9 gives the rear rotor calculated and experimental loads.

From the record of traces, the steady-state value of shear was calculated by measuring the trace displacement, and applying the calibration factor. The trace displacement at 0° and 30° were taken to determine the cosine and sine coefficient of the harmonics. The 0° and 30° positions were located from the timing mark ($\psi = 90^\circ$).

CHAPTER 4

Discussion of Results

A study of the thrust of the rear rotor for $\alpha_R = 5^\circ$, $\theta_R = 10^\circ$, $\alpha_F = 10^\circ$, $\theta_F = 10^\circ$ and for zero, quarter and half radius overlap conditions was carried out. The rotor stagger was kept constant at quarter radius through the study.

Both typical and uniform disc loadings were considered. Figure 13 shows that, at low forward speed ($\mu \leq .10$) there is no difference in the thrust of the rear rotor with either of these loadings, but with $\mu > .10$, a difference exists. Heyson in Ref. 4 has shown that at higher forward speeds, measured downwash along the longitudinal axis shows a better correlation with the theoretical downwash of a uniformly loaded rotor than that of a typically loaded one.

Figure 13 also shows that the thrust of the rear rotor with interference effect is predictable from theory. The thrust without the interference effect, i.e., as a single rotor, was also calculated. The theoretical and experimental results give a good correlation as shown in Fig. 14.

The theoretical steady-state induced velocity ratio $\overline{K}$, used in the calculations and shown in Fig. 15, is the same

at low advance ratio for both types of disc loadings. With the increase of advance ratio, the value of $\overline{K}$ for various overlap condition tends to converge in case of typical disc loading, whereas with uniformly loaded one it increases almost at the same rate with μ . The value of $\overline{K}$ is higher with uniform disc loading at high advance ratio. $\overline{K}$ assumes the value of 1 at $\mu = .25$ and with typical disc loading for all three overlap conditions. But with uniform disc loading $\overline{K}$ varies from 1.1 for zero overlap to 1.45 for half radius overlap.

The procedure followed to obtain the experimental results, Table 11, to study the third harmonic interference effect on the rear rotor due to the front rotor, was not a very accurate one. With the blade pitch of the rear rotor set at 0°, there will be harmonic vibratory forces set up due to the induced steady-state thrust. Hence, the recorded vibratory forces will consist of vibratory forces due to the steady-state thrust of the rear rotor as well as those due to the front rotor downwash.

This explains why no correlation was found between the theoretical and experimental results, Table 11. However, the harmonic analysis of the theoretical front rotor downwash reveals the presence of a strong third harmonic at all overlap conditions.

CHAPTER 5

Conclusion and Recommendations

A theoretical and experimental study of the interference effect on the rear rotor due to the front rotor has been carried out. Although comprehensive conclusions can not be drawn without additional study of the effect of several other parameters, a few concluding remarks are in order on the basis of the work reported herein.

(1) The thrust of the rear rotor (or steady-state induced velocity ratio) in a tandem helicopter can be predicted to a reasonable extent from the charts of Ref. 1. For a given rotor stagger, the thrust varies inversely with the rotor overlap.

(2) Uniform disc loading gives a higher value of $\overline{K}$ than the typical disc loading at high advance ratio. With half radius overlap at $\mu = .25$, $\overline{K}$ assumes a value of 1.45.

Tests should be made for tandem rotors under various operating conditions, so that $\overline{K}$ can be expressed by an empirical equation.

(3) To obtain the third harmonic interference effect on the rear rotor experimentally, its steady-state thrust must be zero. This can be achieved by setting the pitch of the rear rotor blade to cancel the effect of the front rotor steady-state downwash. Further tests with this pitch will be of interest.

(4) In a tandem set-up, the induced third harmonic downwash at the rear rotor is very strong. It may be worth examining the possibility of using rotors with more than three blades in a tandem rotor helicopter.

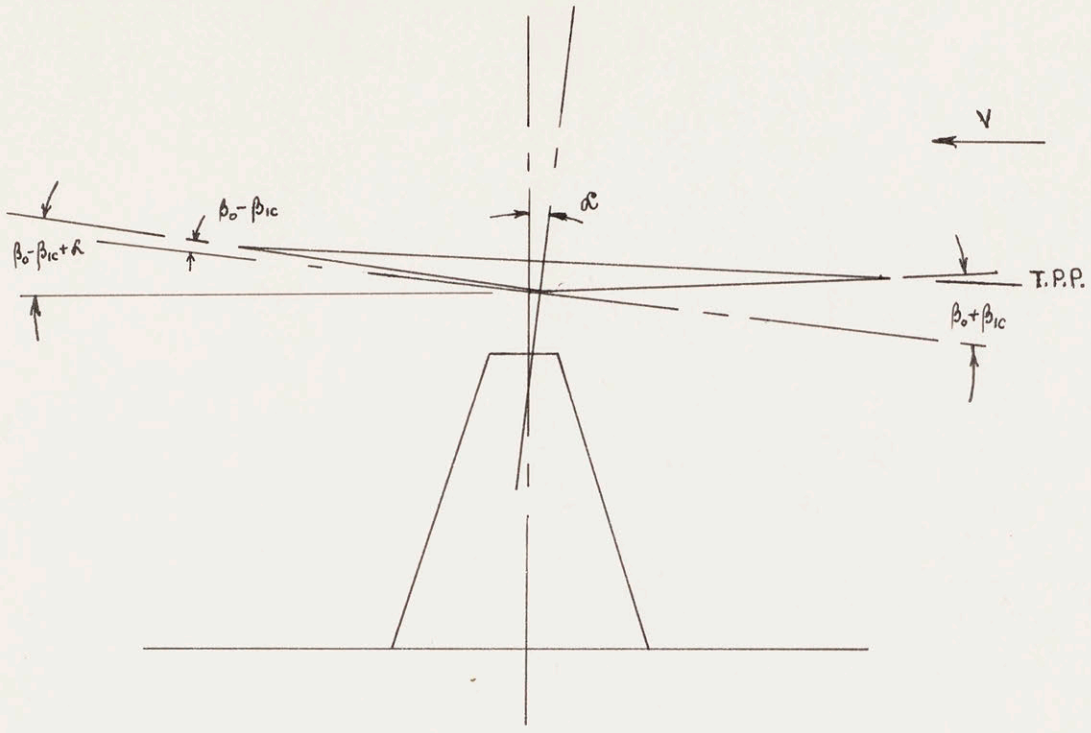

Fig. 1. Single Rotor Geometry.

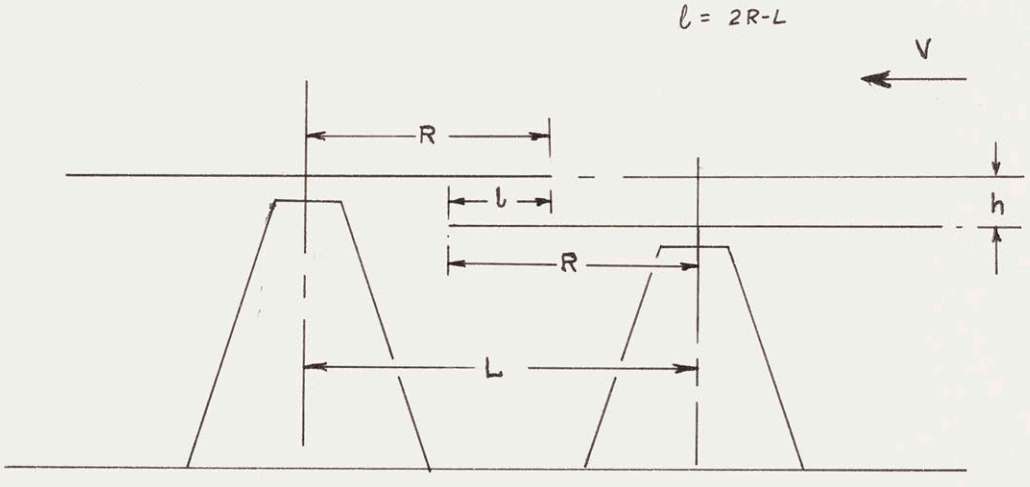

Fig. 2. Tandem Rotor Geometry.

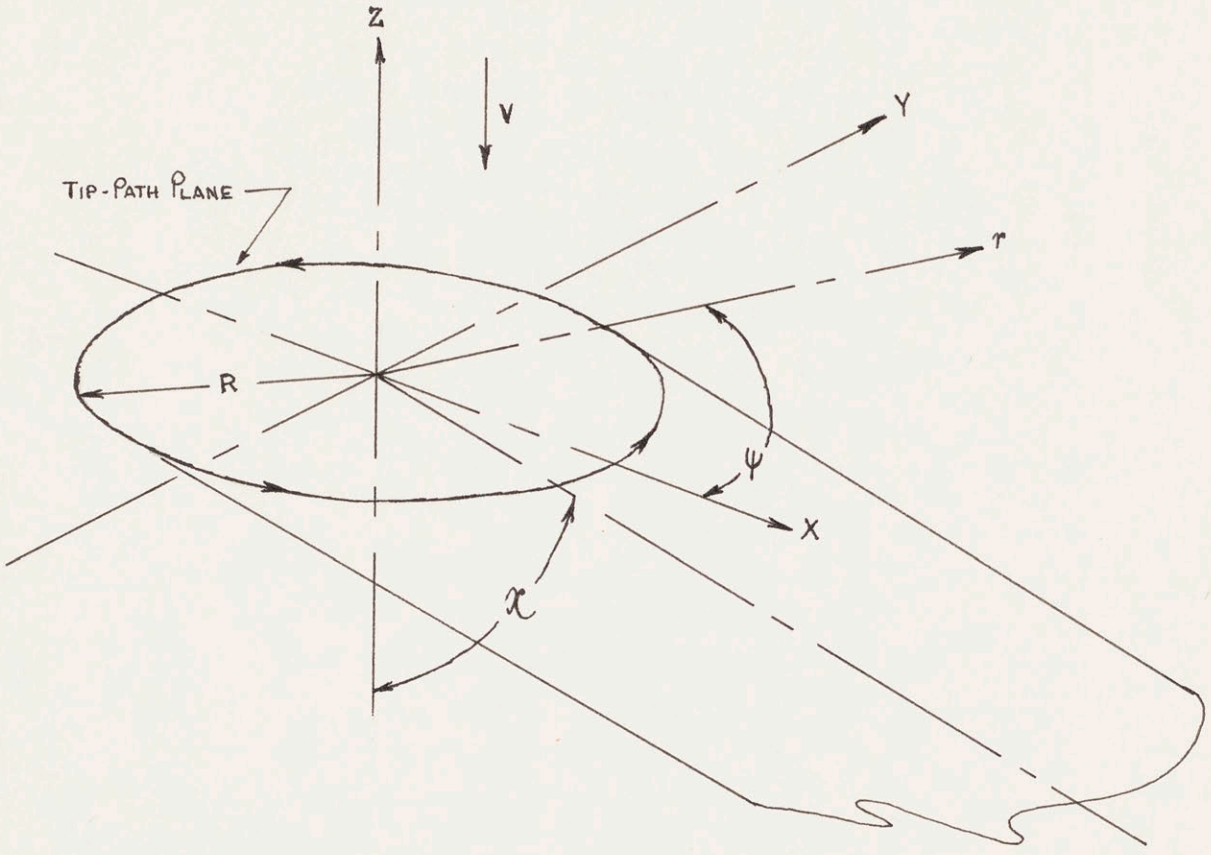

Fig. 3 - Geometry of Wake - Arrows Denote Positive Direction

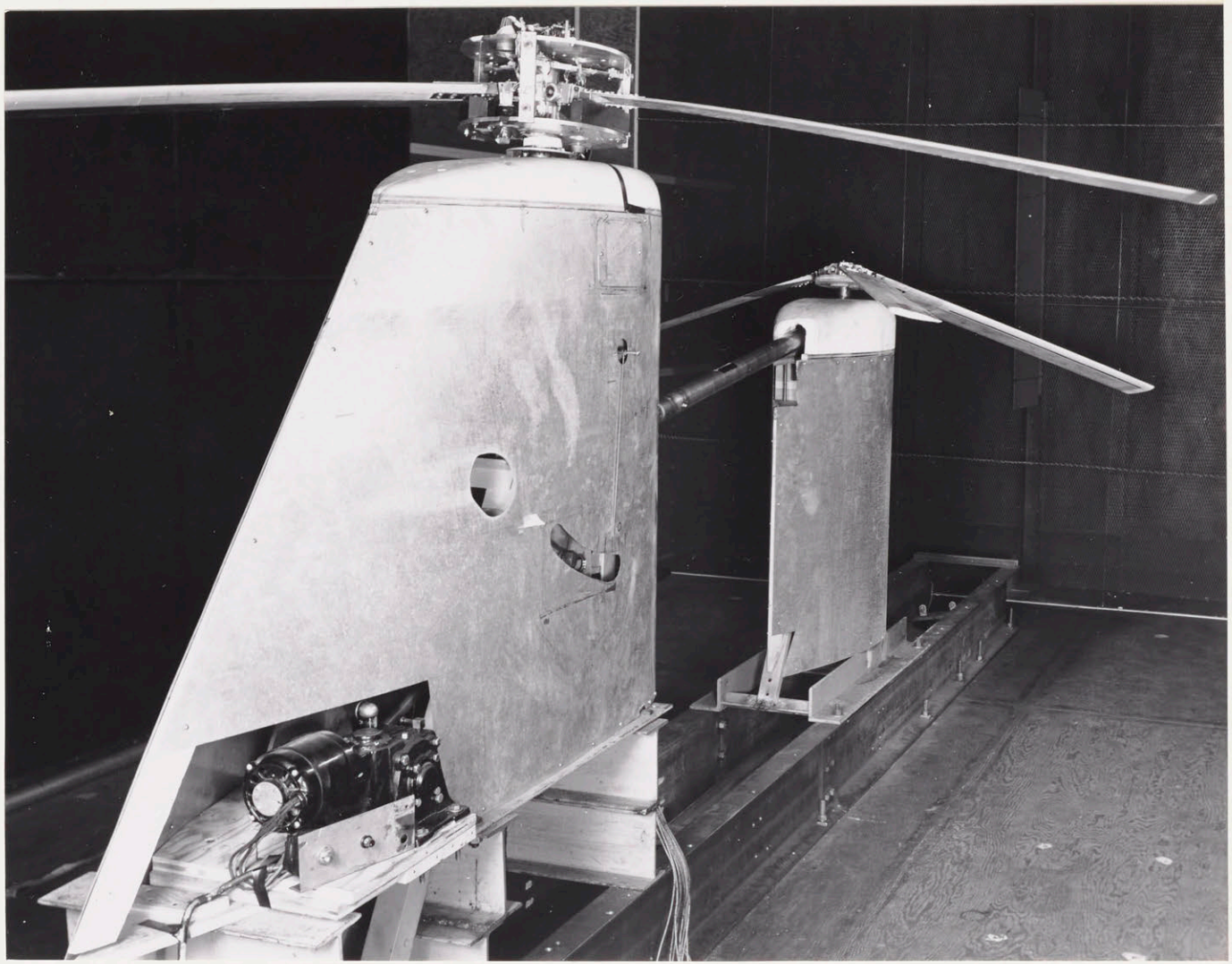

Fig. 4 Tandem Rotor Pylons

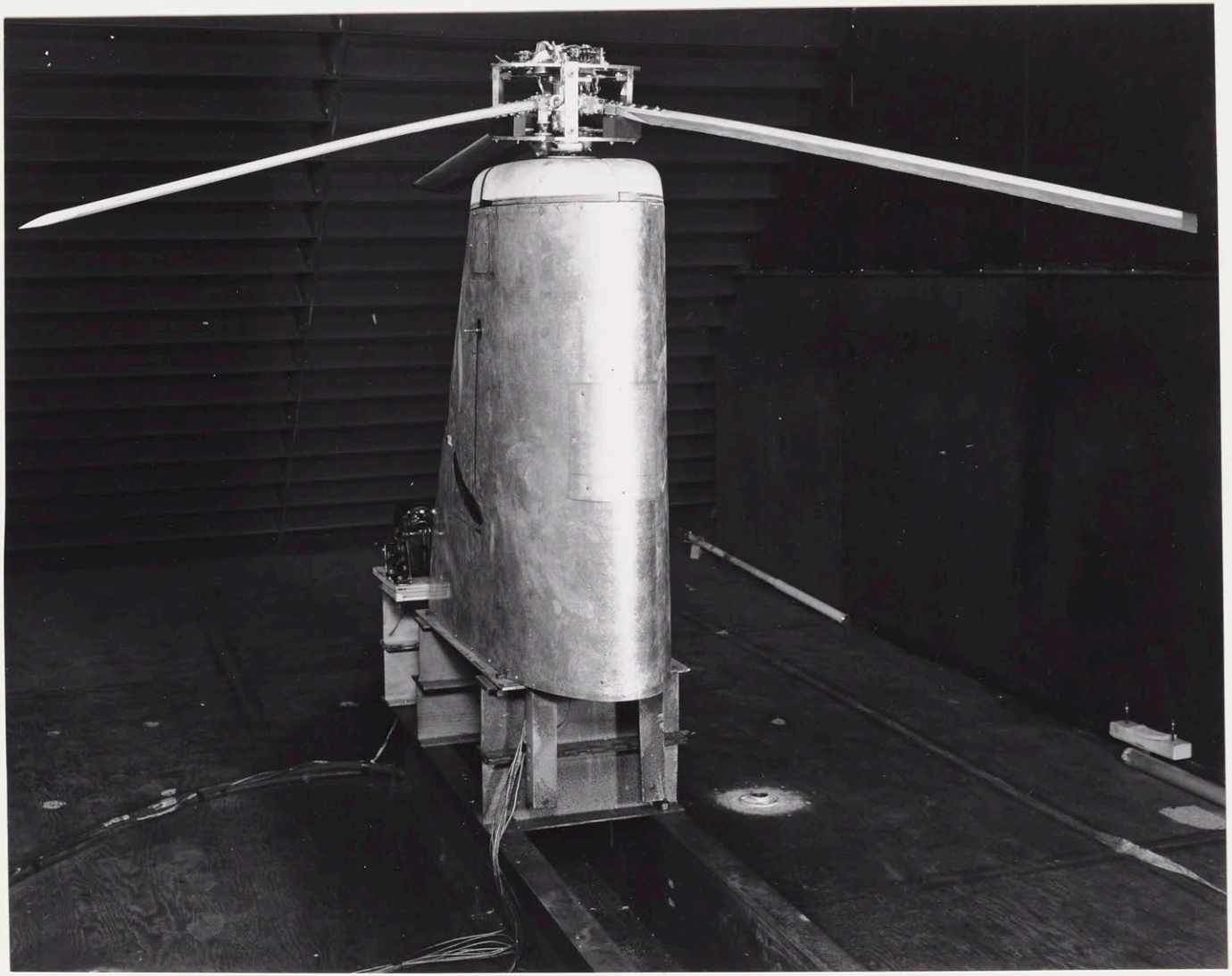

Fig. 5 Single Rotor Setup

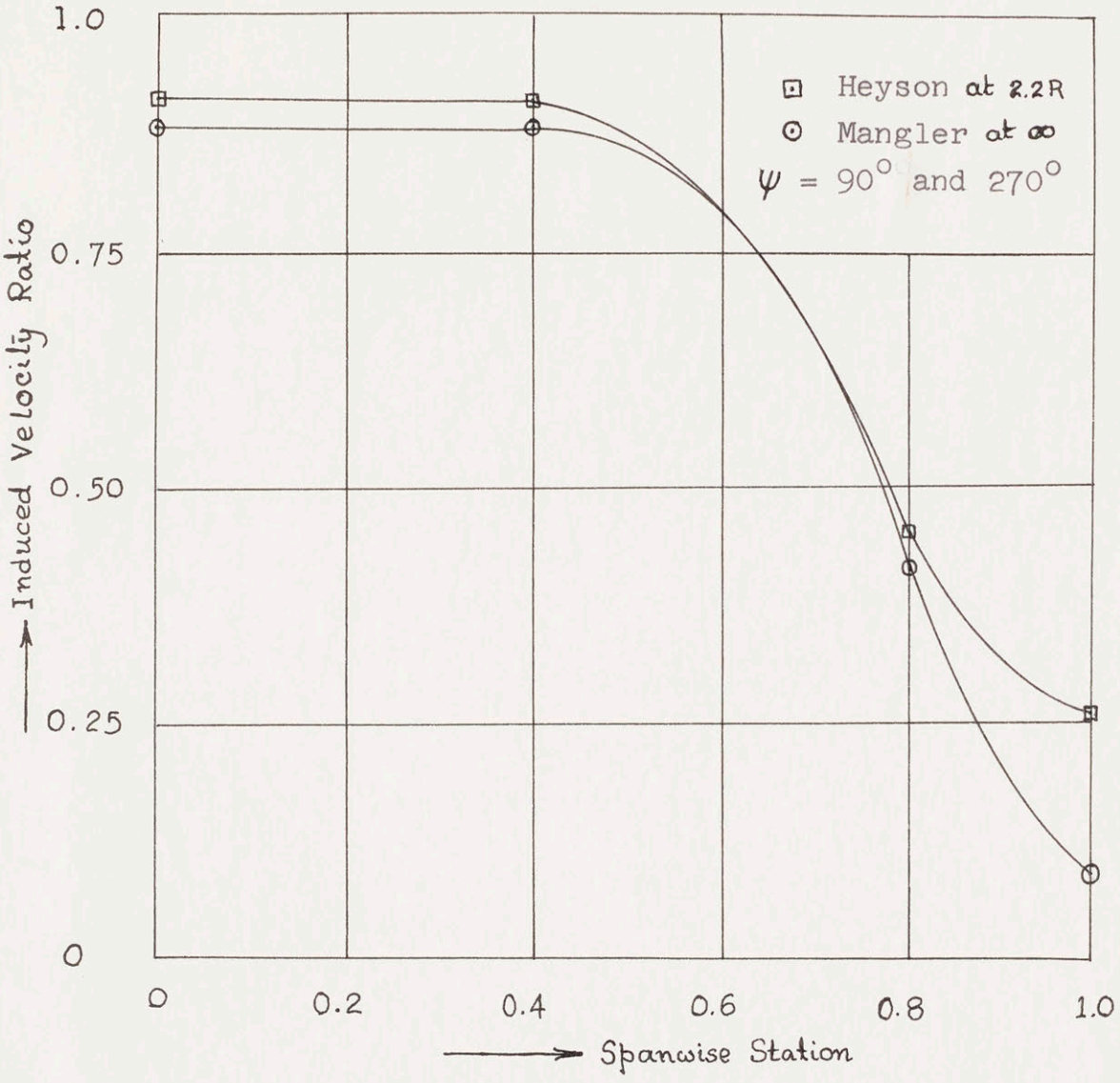

Fig. 6. Contour of Induced Velocity Ratio for a Wake Angle of 76°, from Heyson and Mangler's Theory.

Wake angle 81.7 ——·—— Wake angle 72.9 ——··——

Wake angle 78.2 ——···—— Wake angle 61.5 ——·——

Wake angle 36.9 ——

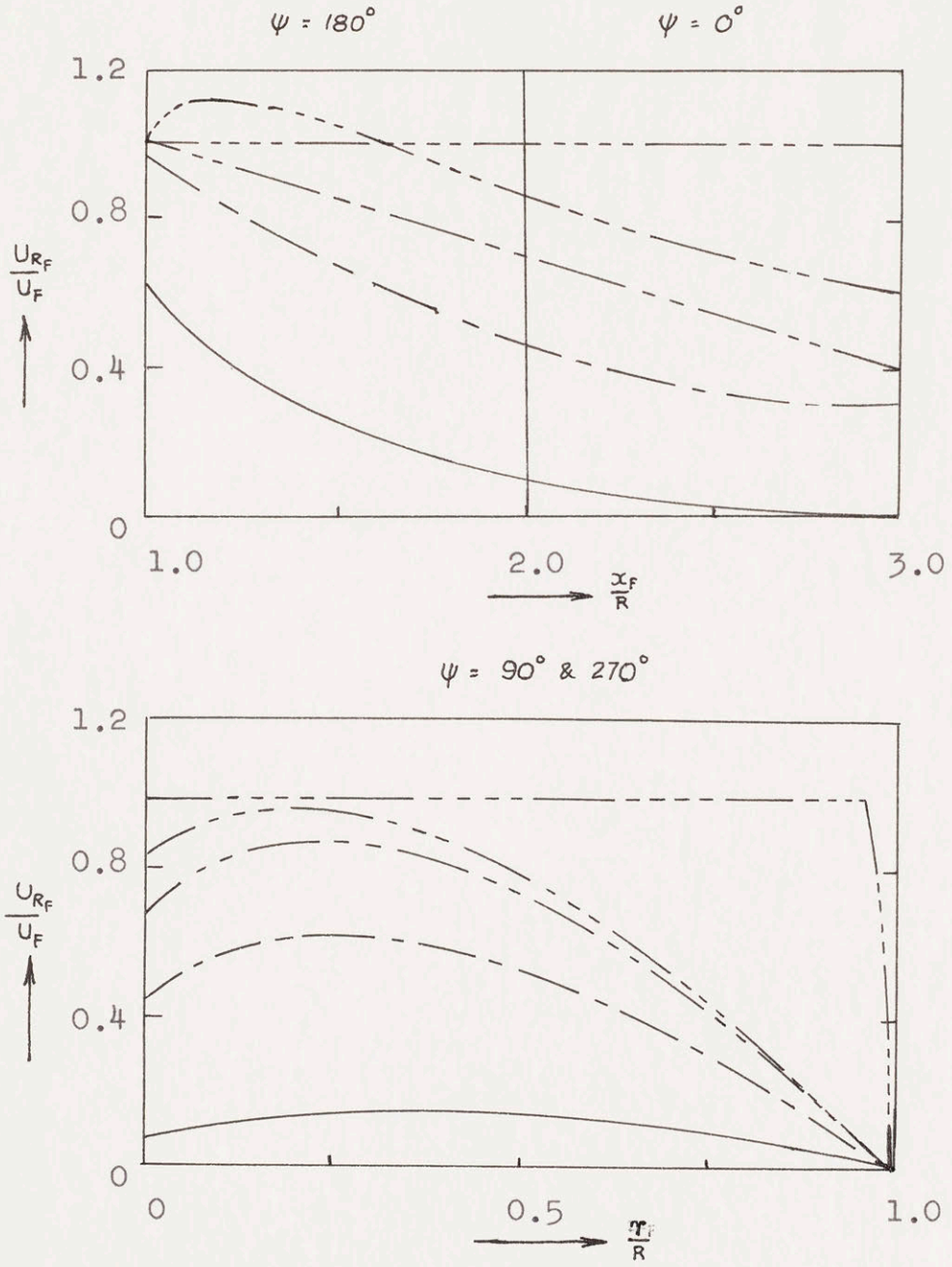

Fig. 7. Induced-Velocity Distribution Along the Longitudinal and the Lateral Axis

(Typical Disc Loading)

l/R = 0 h/R = .25

Wake angle 81.7 —·····— Wake angle 72.9 —·-·—

Wake angle 78.2 —·····— Wake angle 61.5 —·-·—

Wake angle 36.9 ——

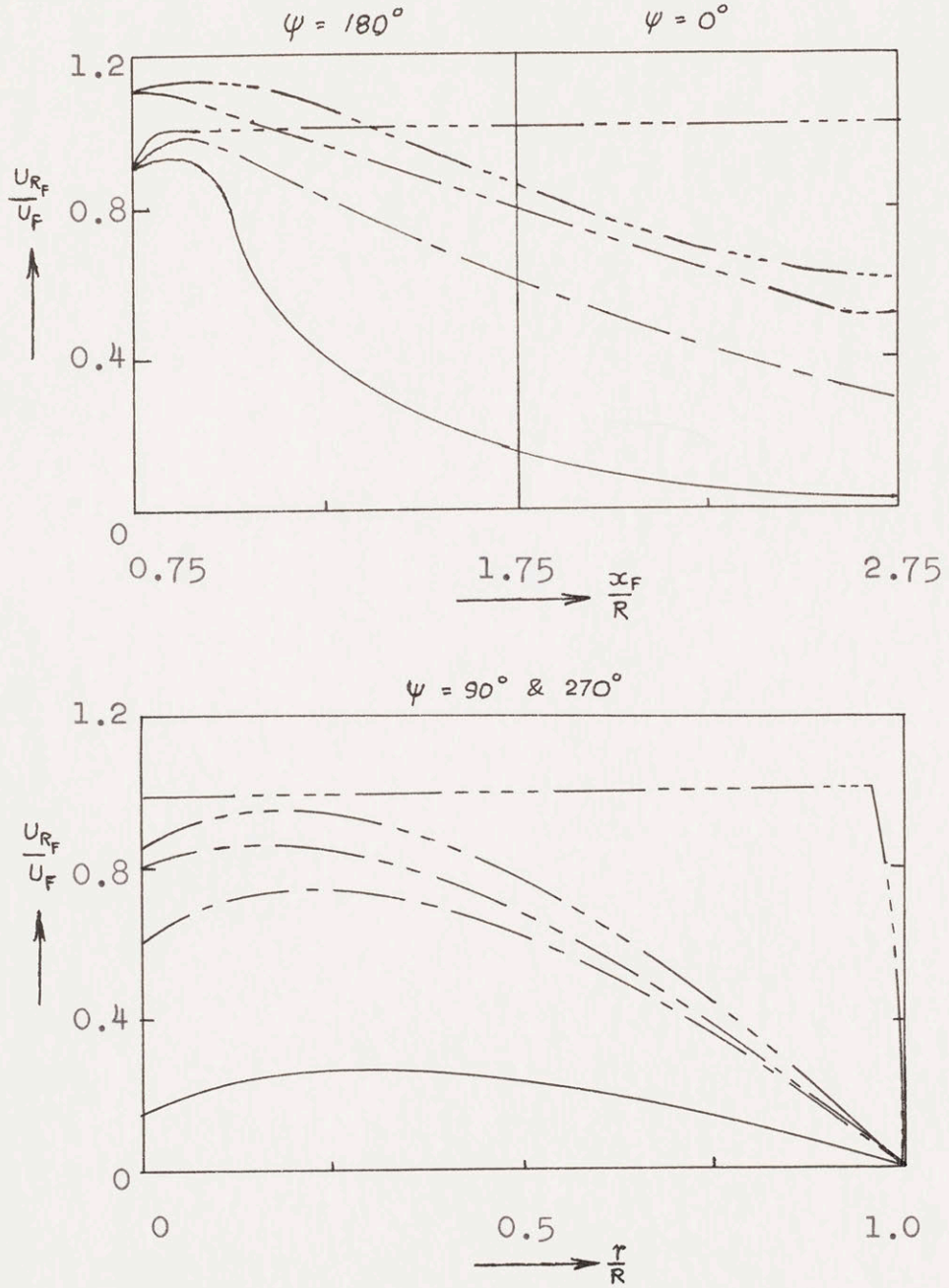

Fig. 8. Induced-Velocity Distribution Along the Longitudinal and the Lateral Axis

(Typical Disc Loading)

l/R = .25 h/R = .25

Wake angle 81.7 ——·—— Wake angle 72.9 ——·—

Wake angle 78.2 ——·—— Wake angle 61.5 ——·—

Wake angle 36.9 ——

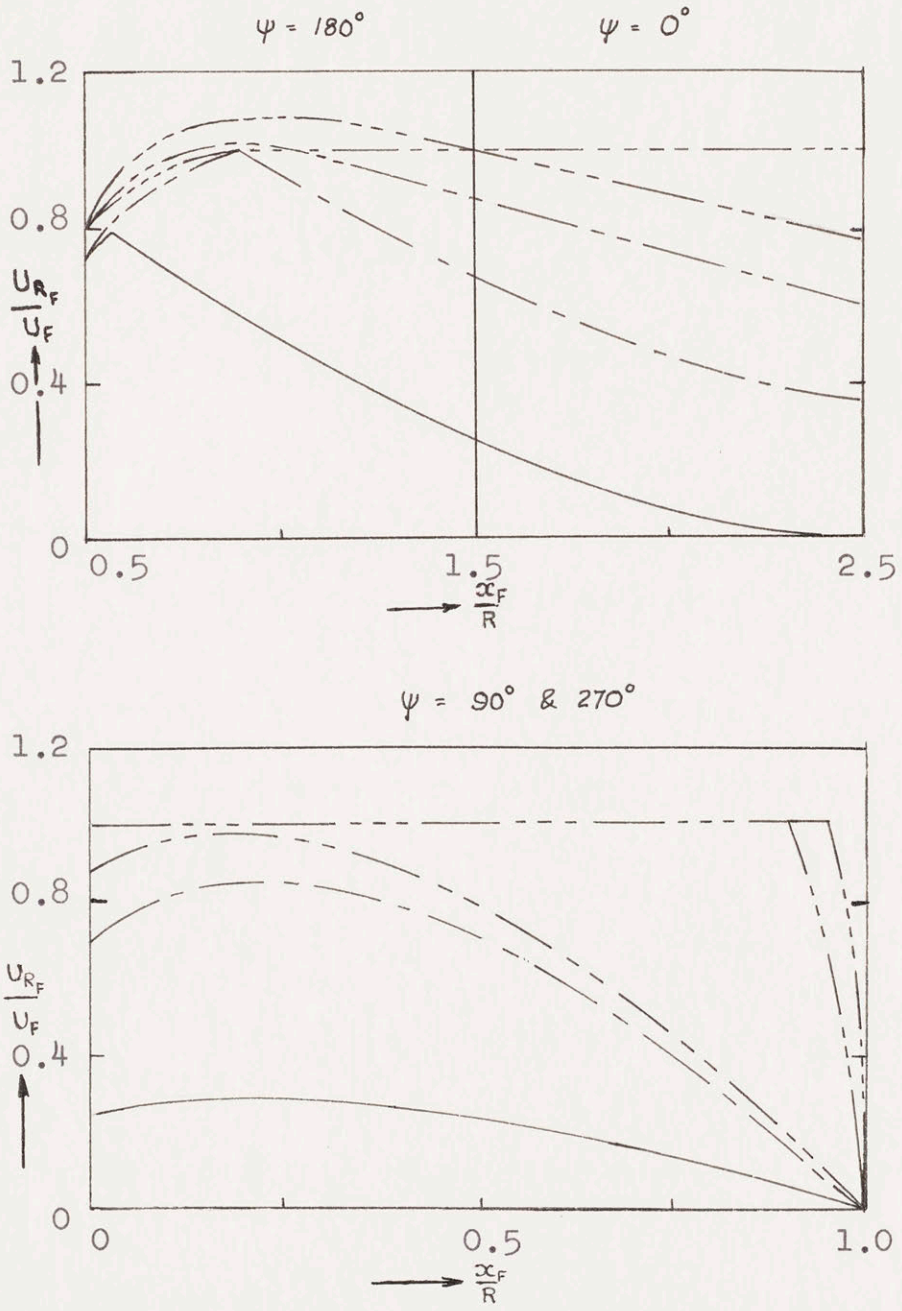

Fig. 9. Induced-Velocity Distribution Along the Longitudinal and the Lateral Axis

(Typical Disc Loading)

l/R = .50 h/R = .25

Wake angle 81.7 ——·—— Wake angle 72.9 ——·—·——

Wake angle 78.2 ——·—·—— Wake angle 61.5 ——·—·——

Wake angle 36.9 ——

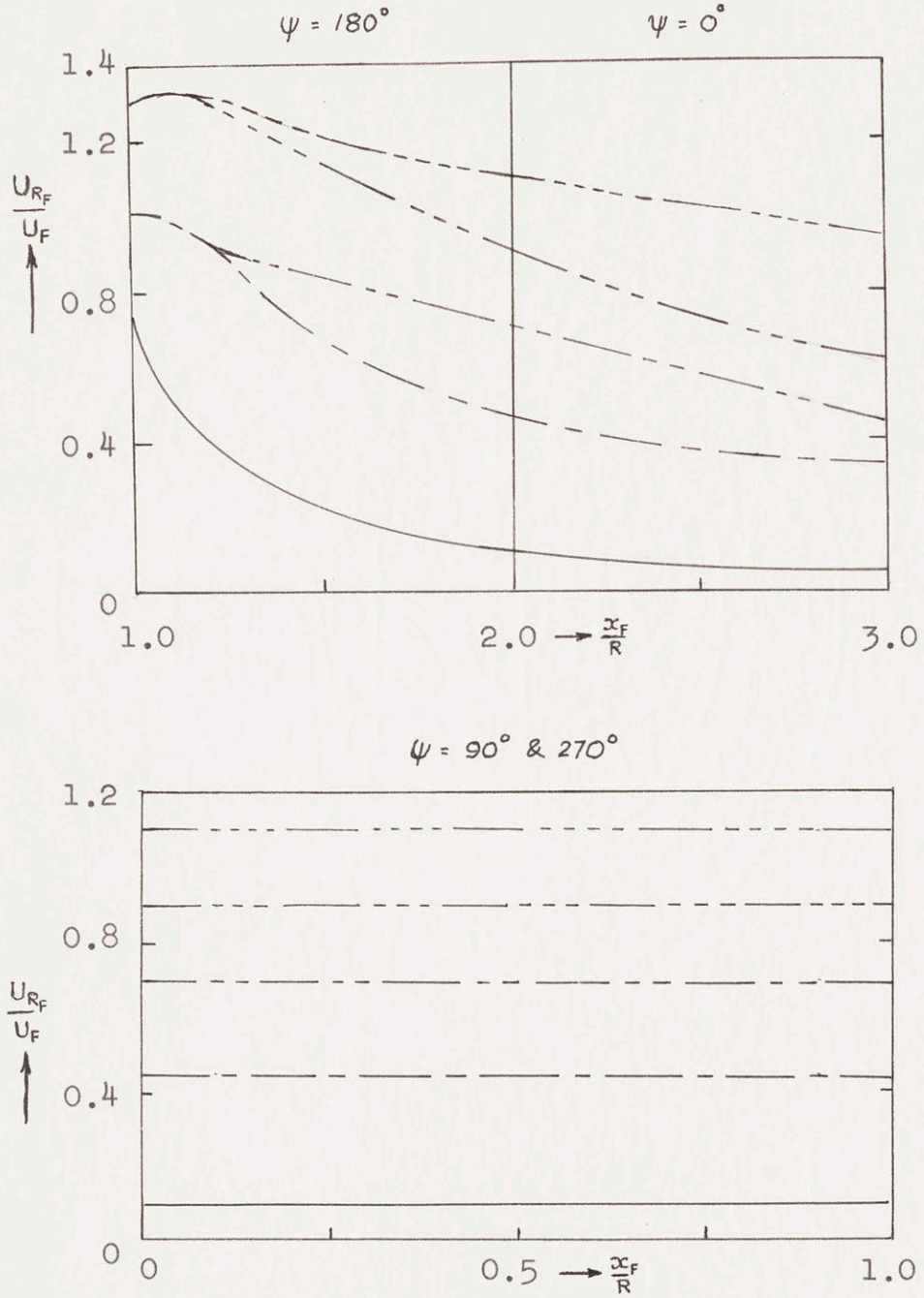

Fig. 10. Induced-Velocity Distribution Along the Longitudinal and the Lateral Axis

(Uniform Disc Loading)

$l/R = 0$ $h/R = .25$

Wake angle 81.7 —·····— Wake angle 72.9 —··—

Wake angle 78.2 —·····— Wake angle 61.5 —·—

Wake angle 36.9 ——

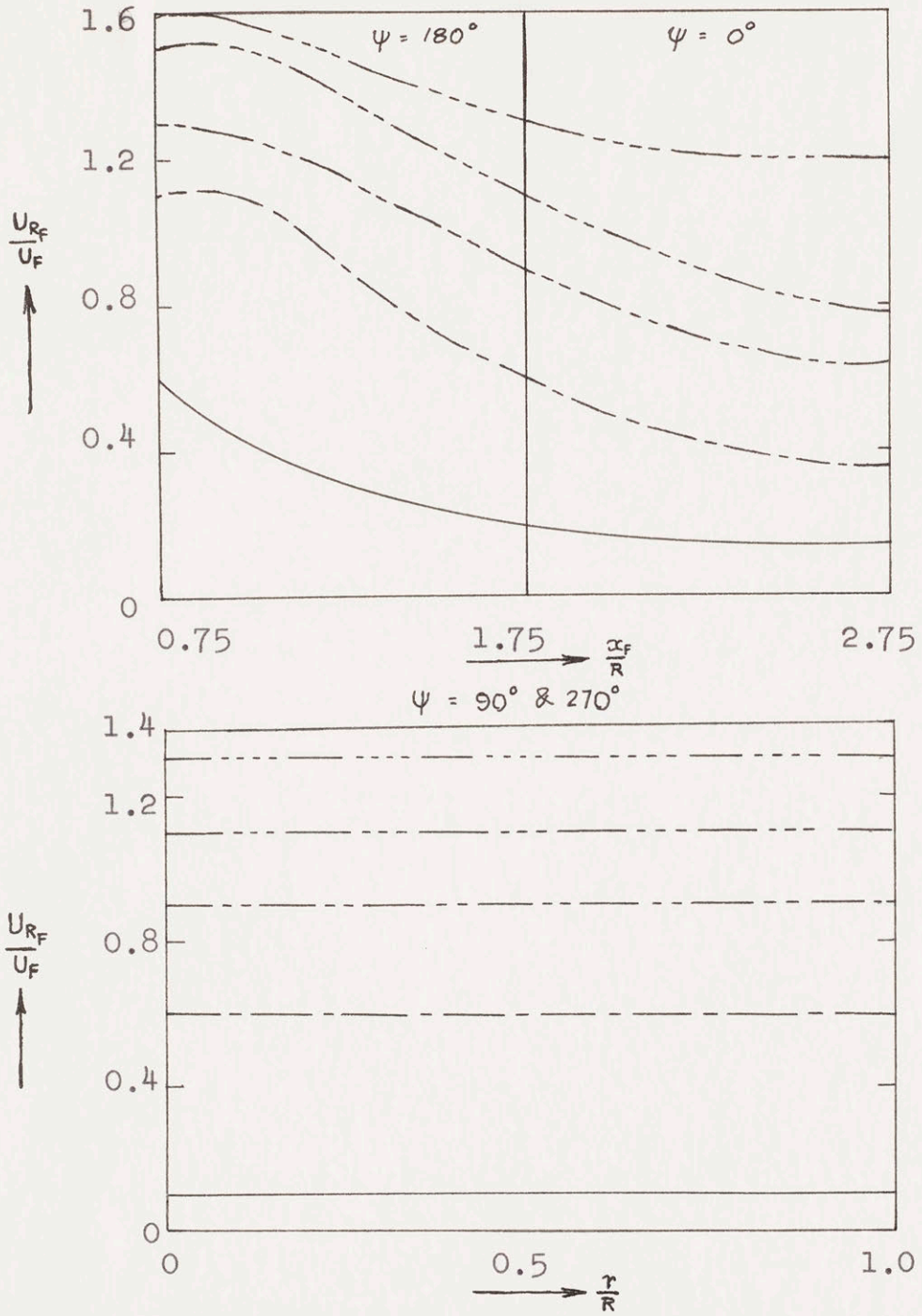

Fig. 11. Induced-Velocity Distribution Along the Longitudinal And the Lateral Axis

(Uniform Disc Loading)

$l/R = .25$ $h/R = .25$

Wake angle 81.7 ------ Wake angle 72.9 ---- Wake angle 78.2 ------ Wake angle 61.5 ---- Wake angle 36.9 ——

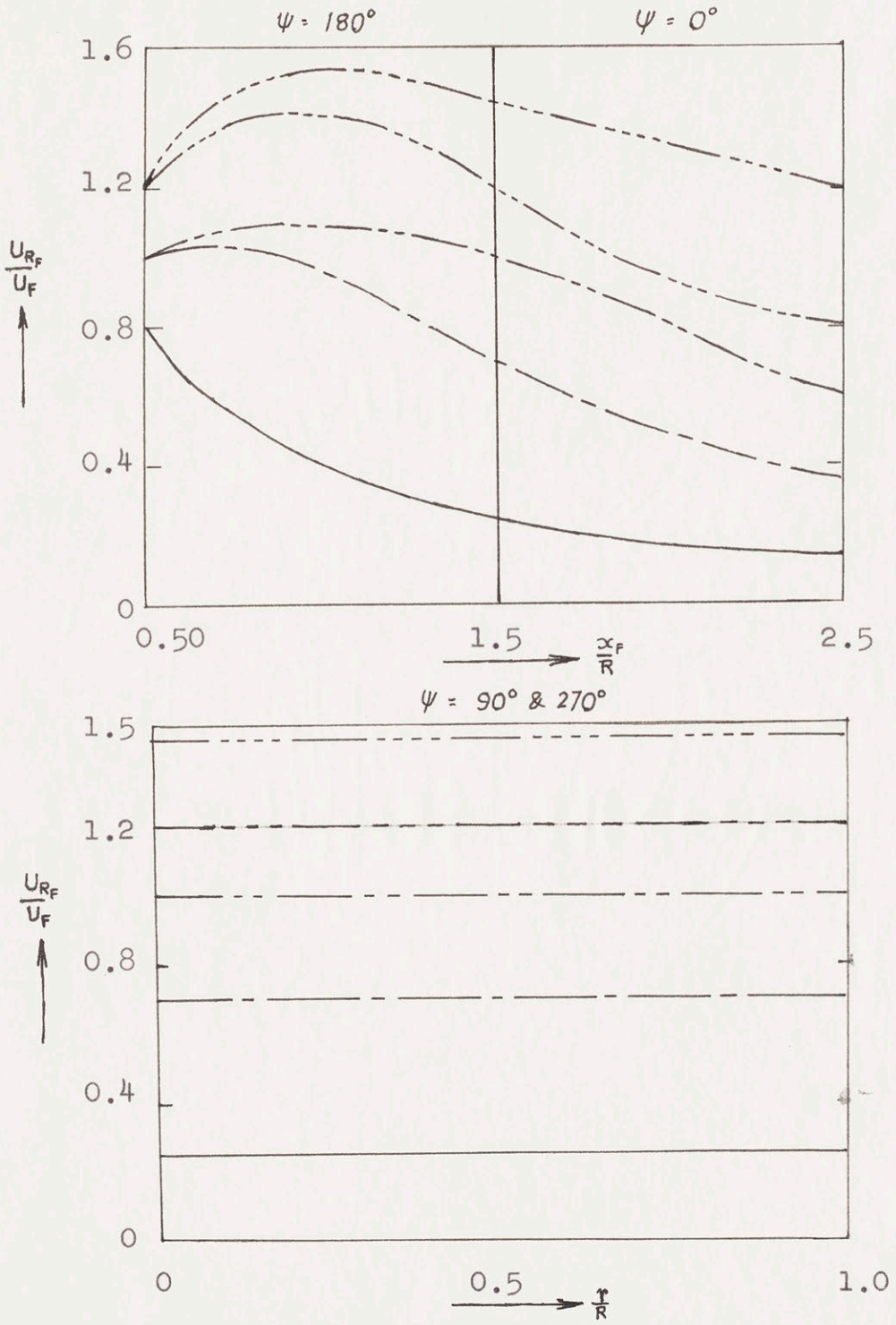

Fig. 12. Induced-Velocity Distribution Along the Longitudinal and the Lateral Axis

(Uniform Disc Loading)

l/R = .50 h/R = .25

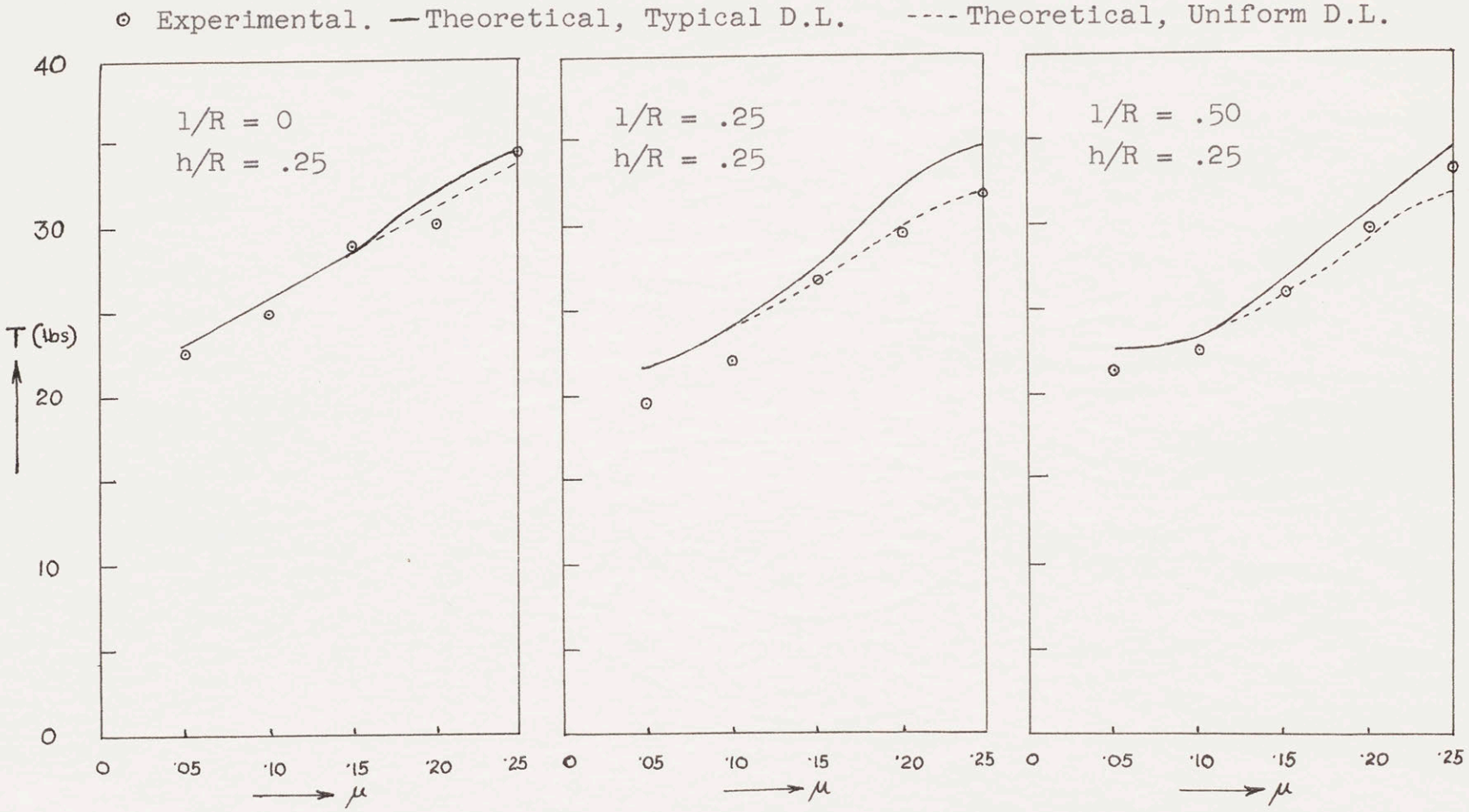

Fig. 13. Rear Rotor Thrust for Various Overlap and Forward Speed

$\alpha_F = 5^\circ$ $\theta_F = 10^\circ$ $\alpha_R = 10^\circ$ $\theta_R = 10^\circ$ N = 400 rpm

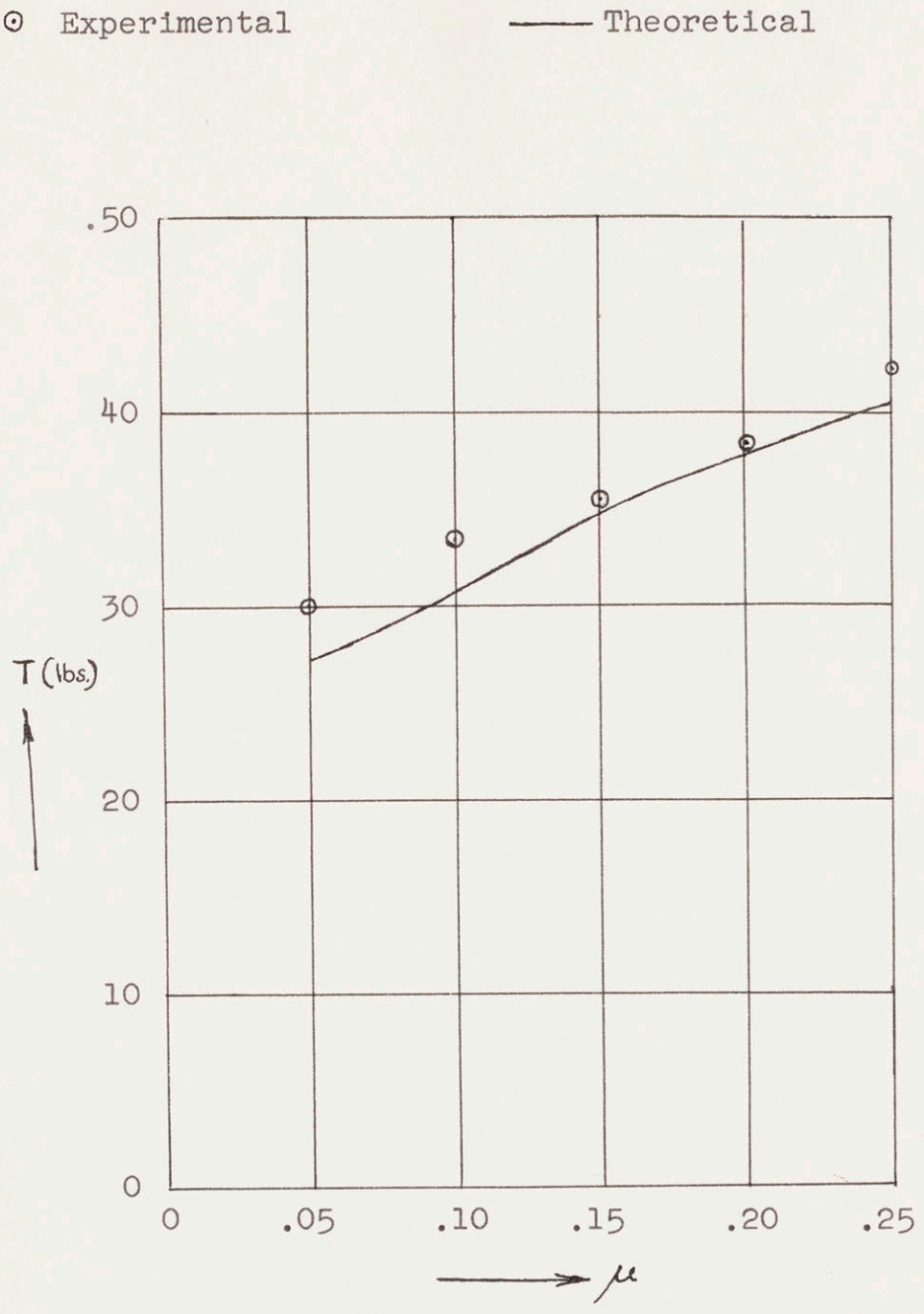

Fig. 14. Theoretical and Experimental Values of Rear Rotor Thrust Without Interference Effects

Typical Disc Loading

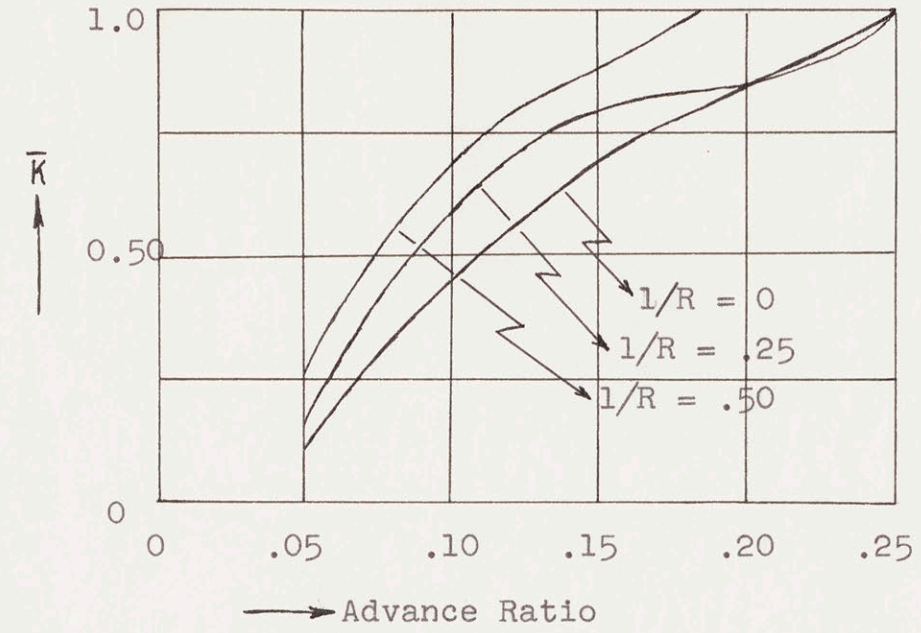

Uniform Disc Loading

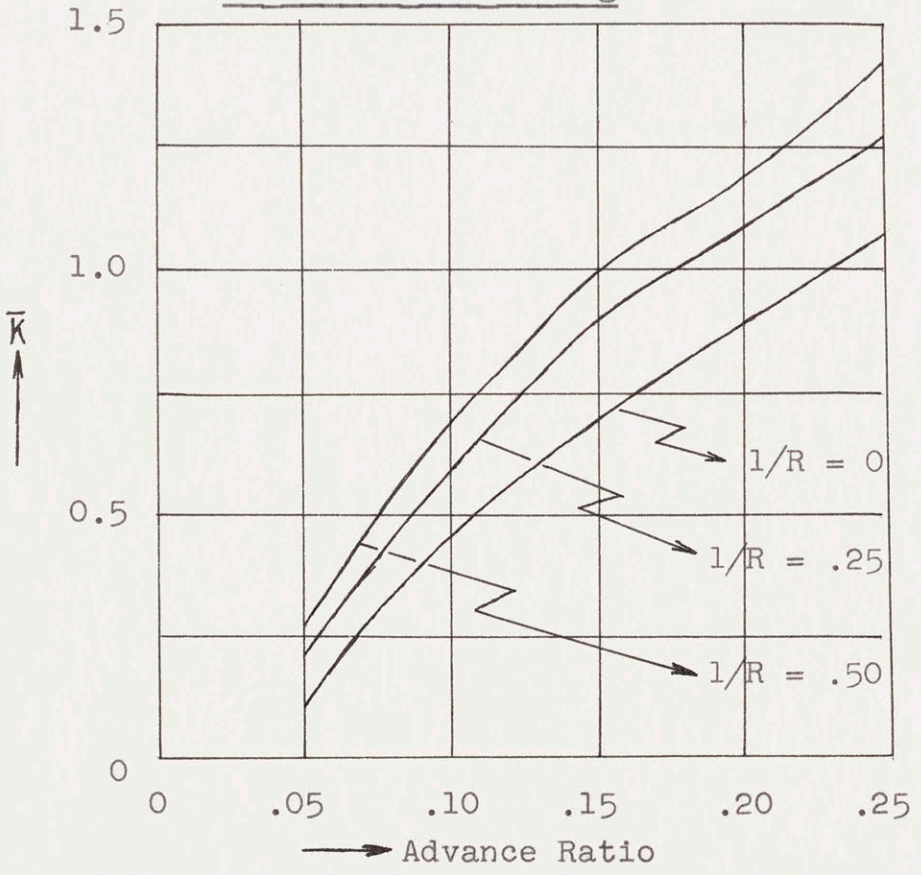

Fig. 15. Induced Velocity Ratio Versus Advance Ratio

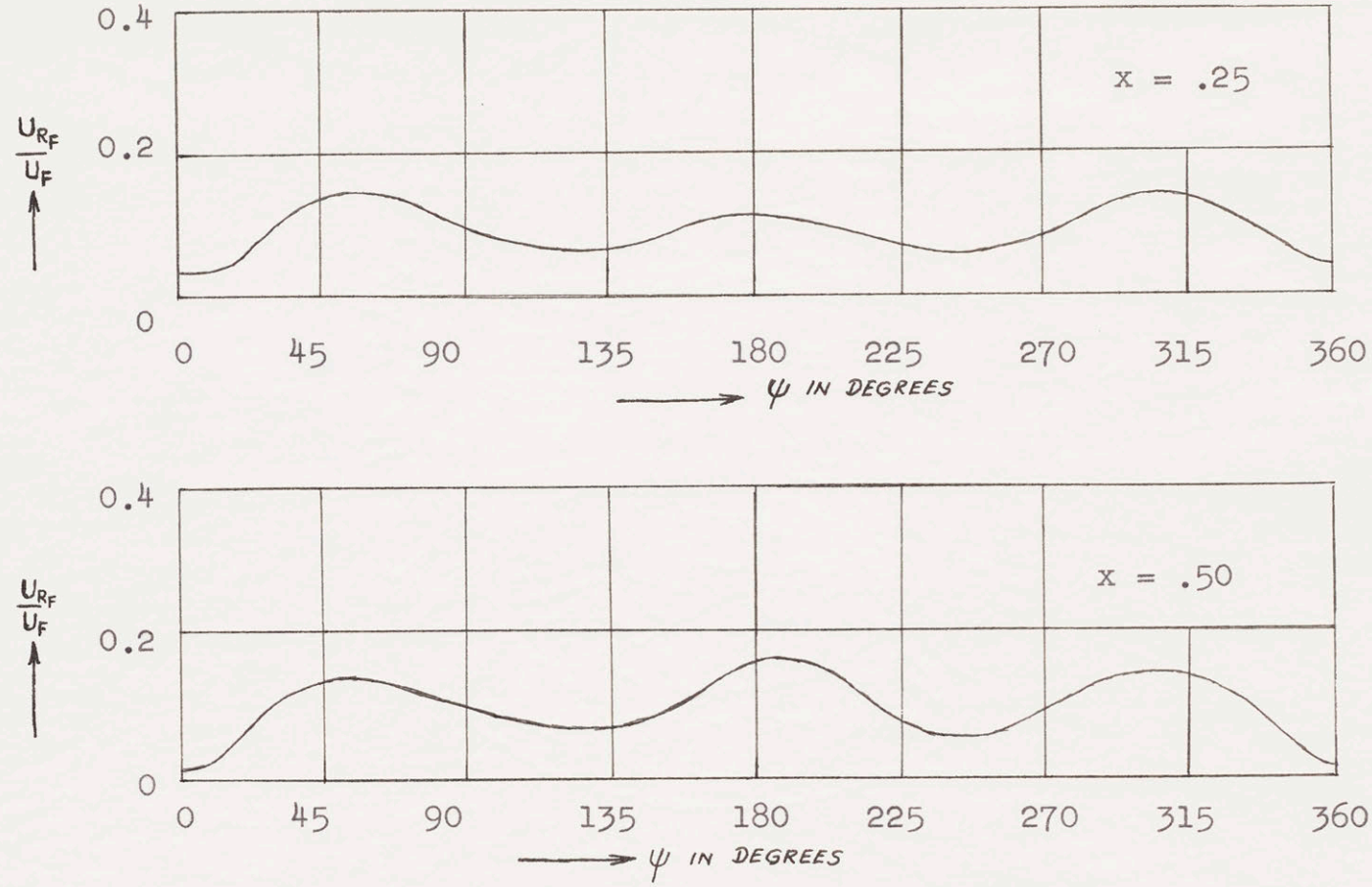

Fig. 16. Induced Velocity Ratio Versus Azimuth (1/R = 0, h/R = .25, μ = .05)

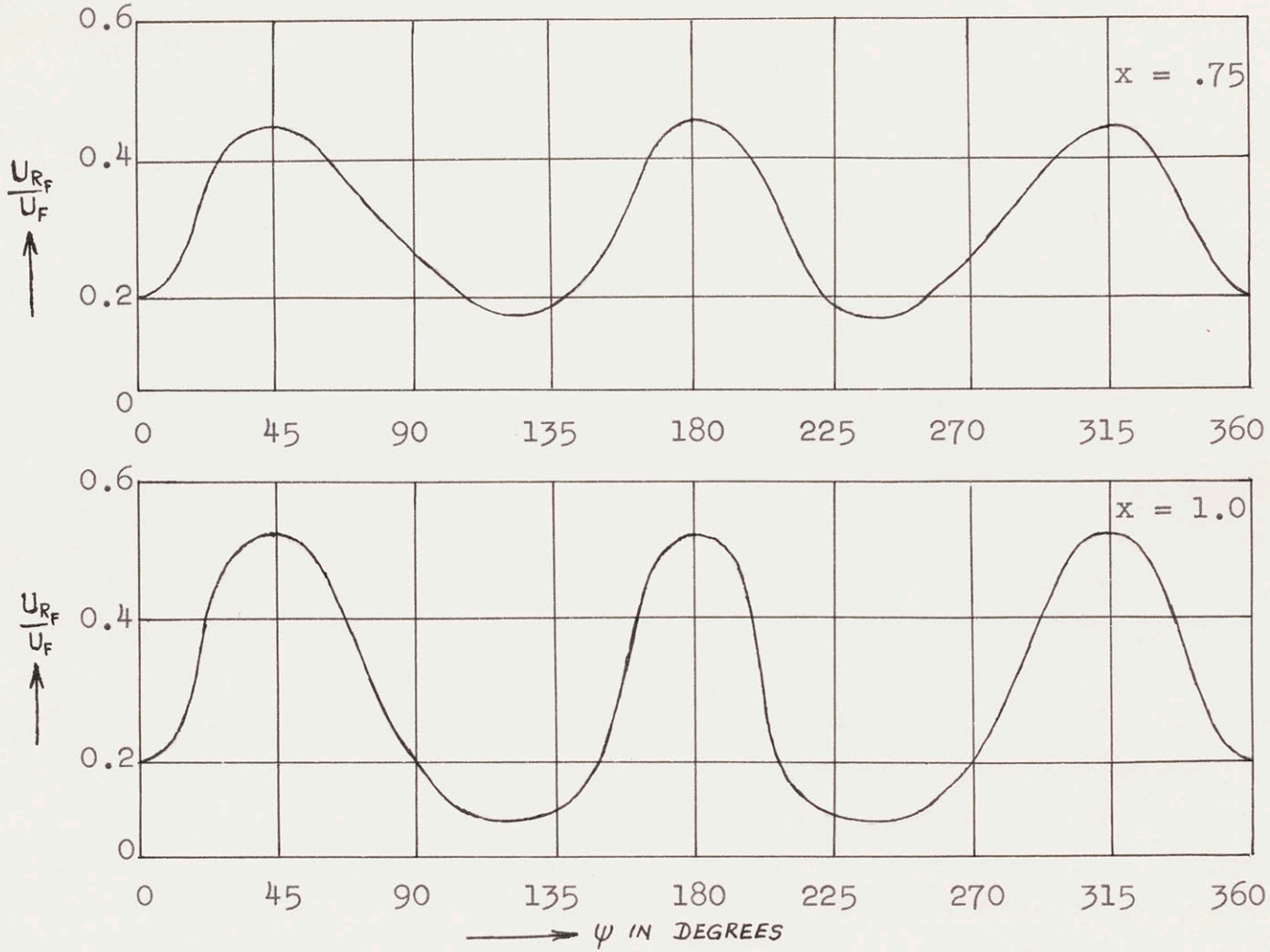

Fig. 17. Induced Velocity Ratio Versus Azimuth (1/R = 0, h/R = .25, μ = .05)

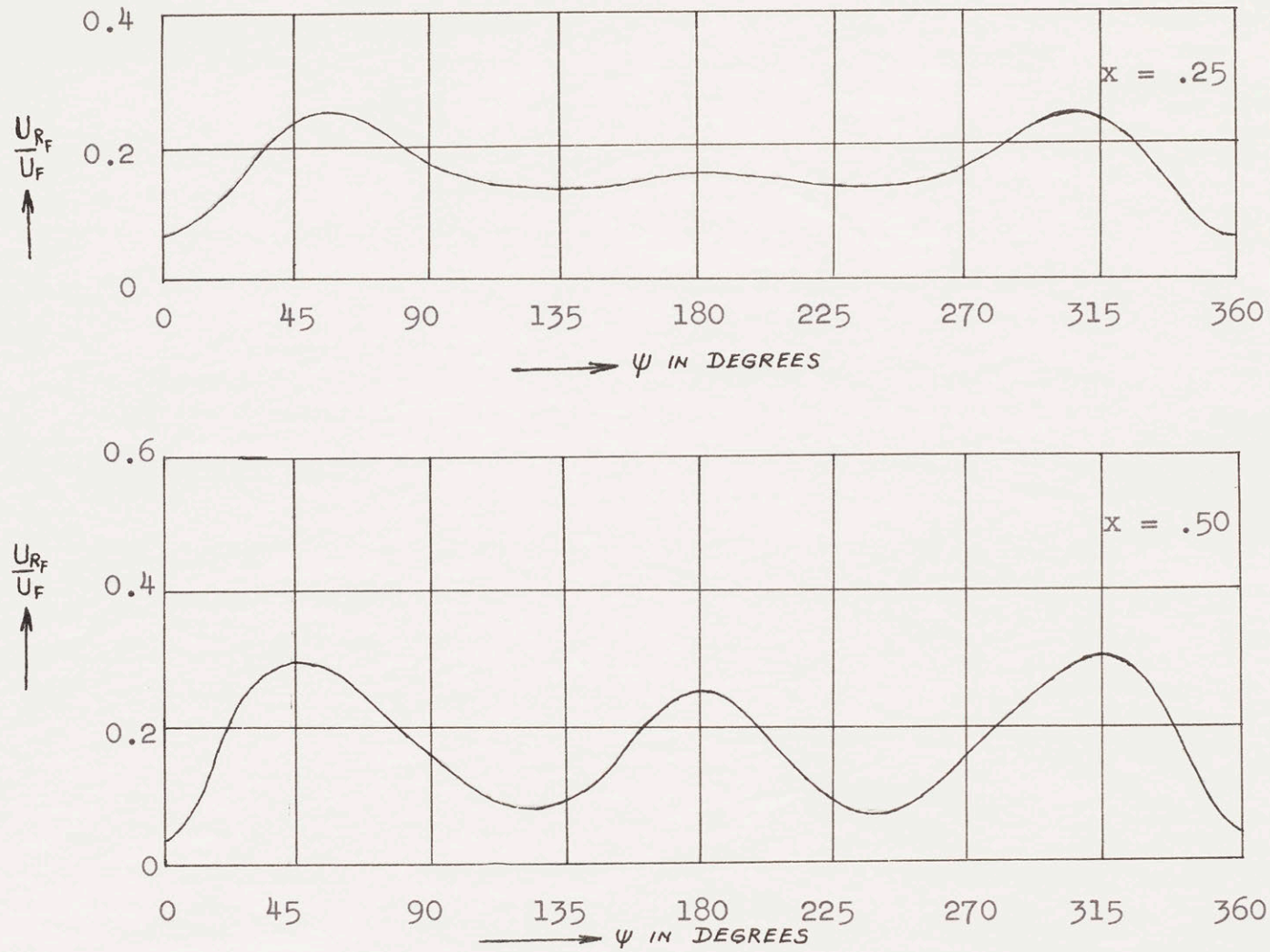

Fig. 18. Induced Velocity Ratio Versus Azimuth (1/R = .25, h/R = .25, μ = .05)

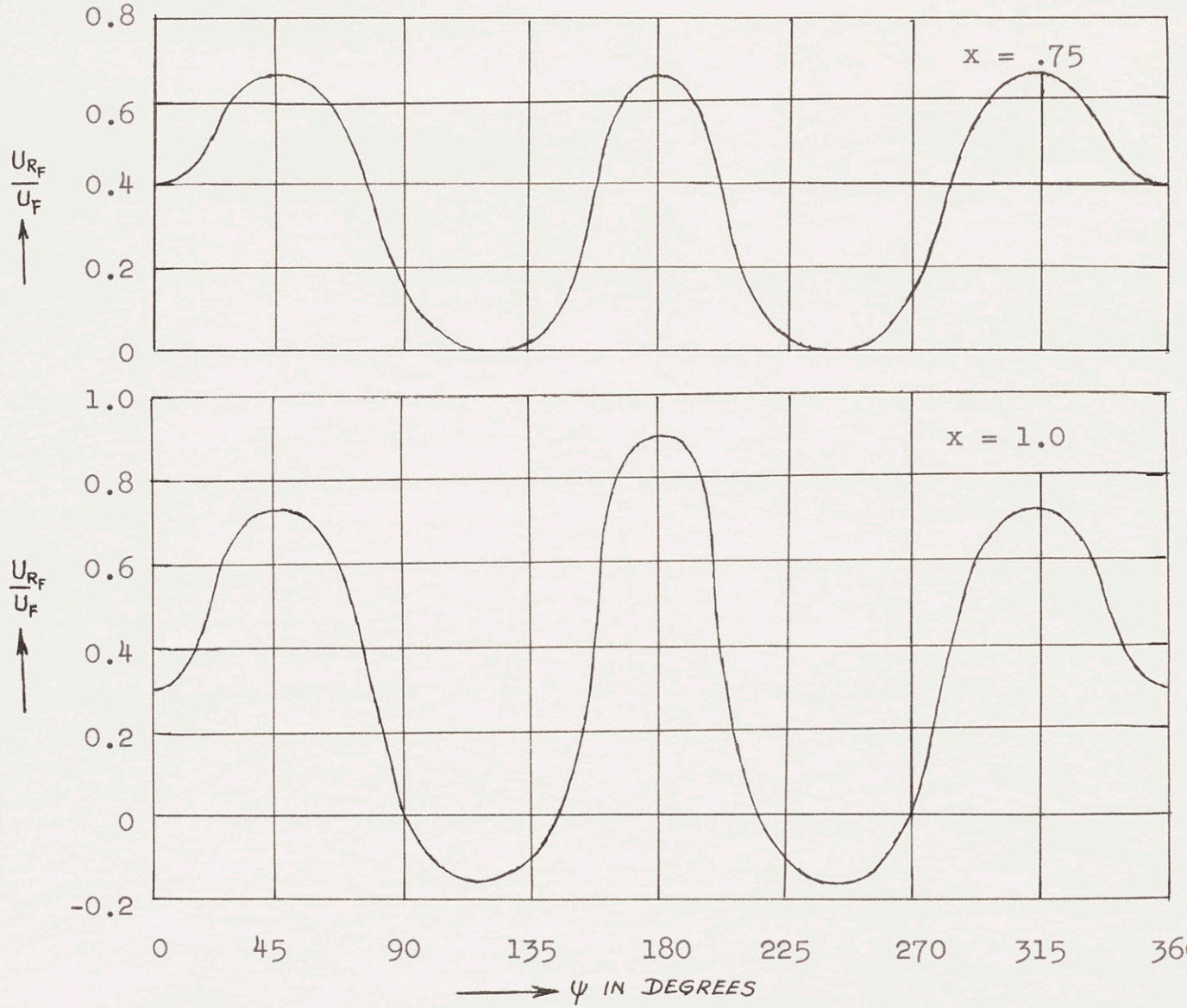

Fig. 19. Induced Velocity Ratio Versus Azimuth (1/R = .25, h/R = .25, μ = .05)

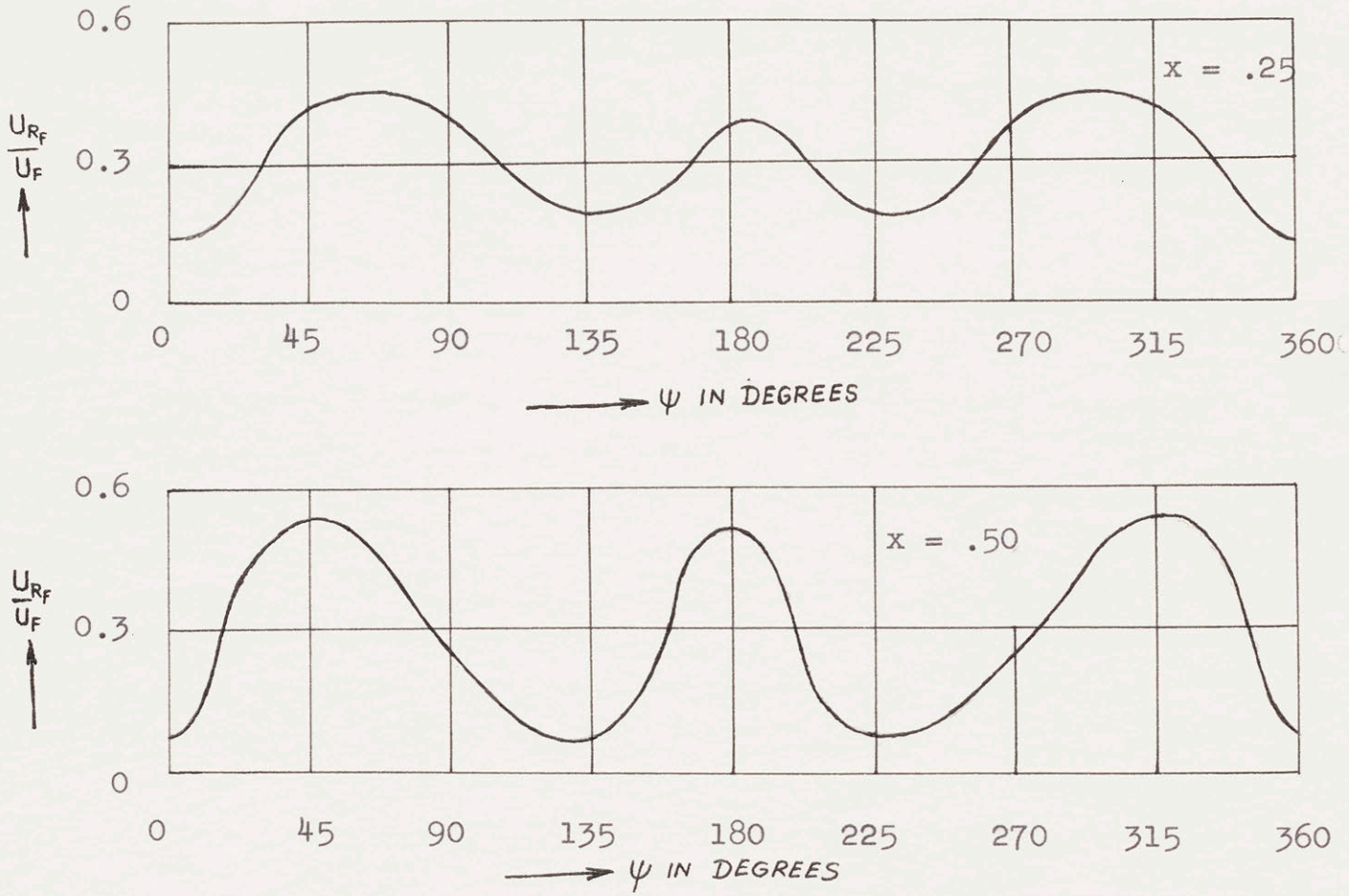

Fig. 20. Induced Velocity Ratio Versus Azimuth (1/R = .50, h/R = .25, μ = .05)

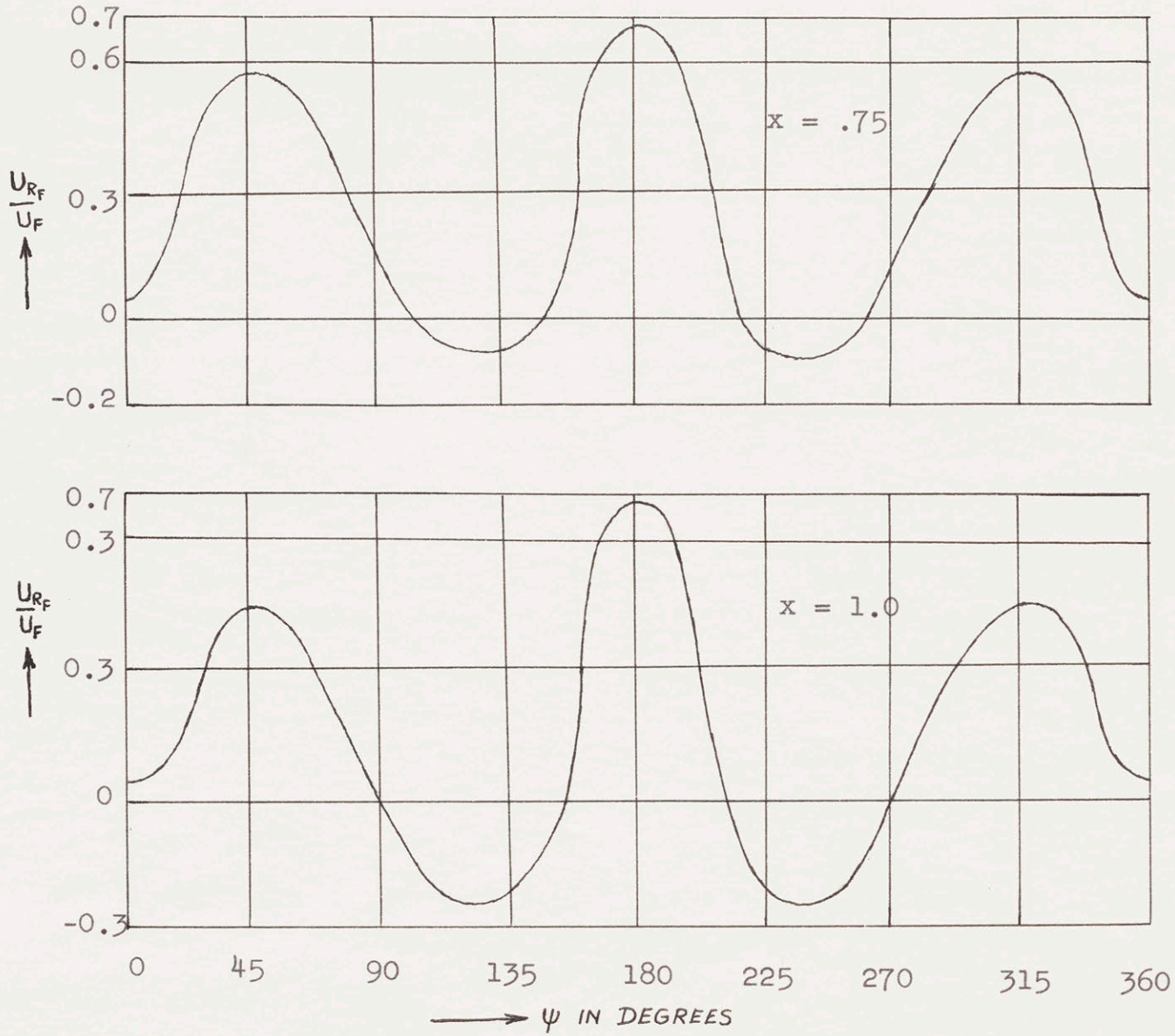

Fig. 21. Induced Velocity Ratio Versus Azimuth (l/R = .50, h/R = .25, μ = .05)

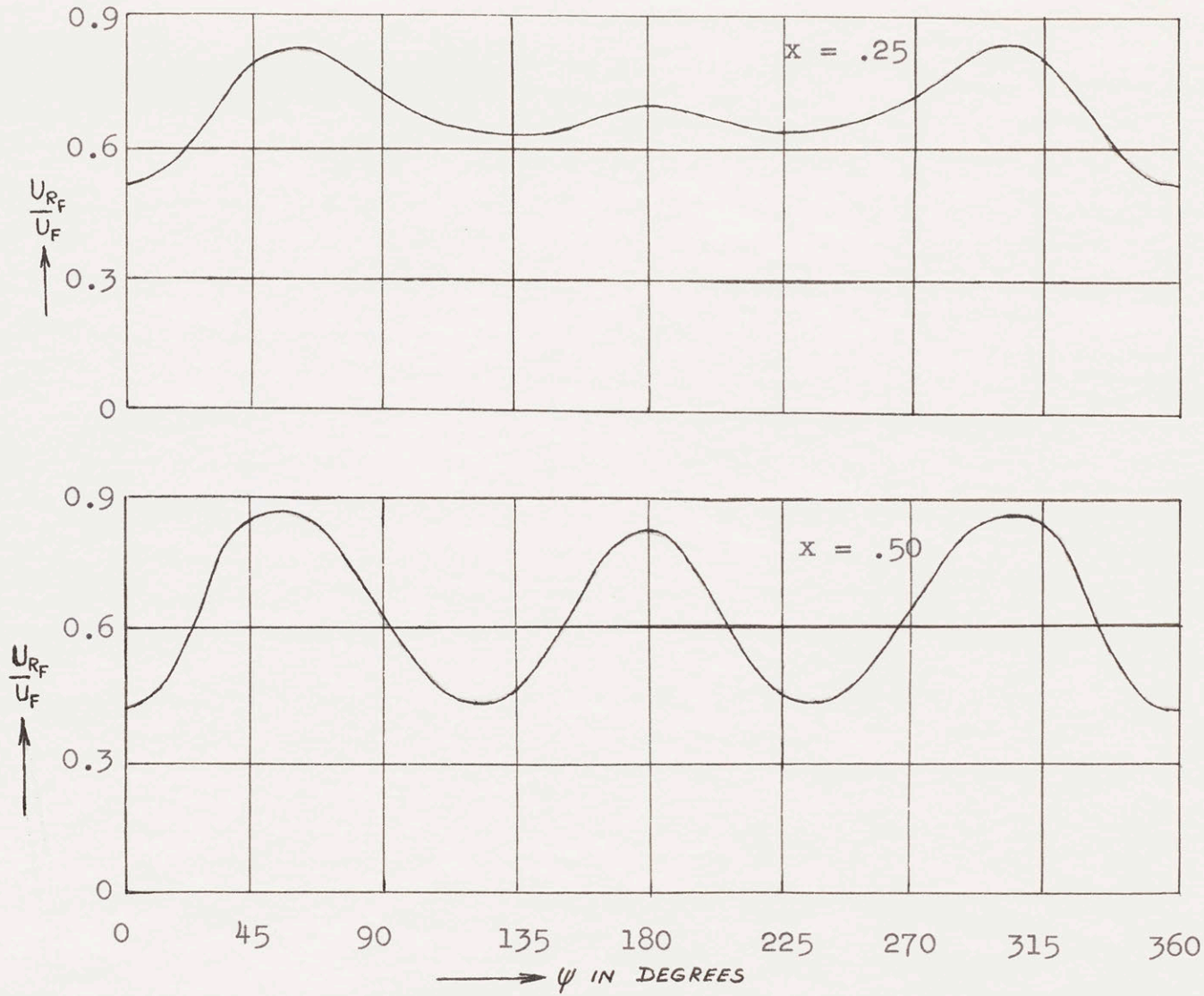

Fig. 22. Induced Velocity Ratio Versus Azimuth (l/R = .25, h/R = .25, μ = .10)

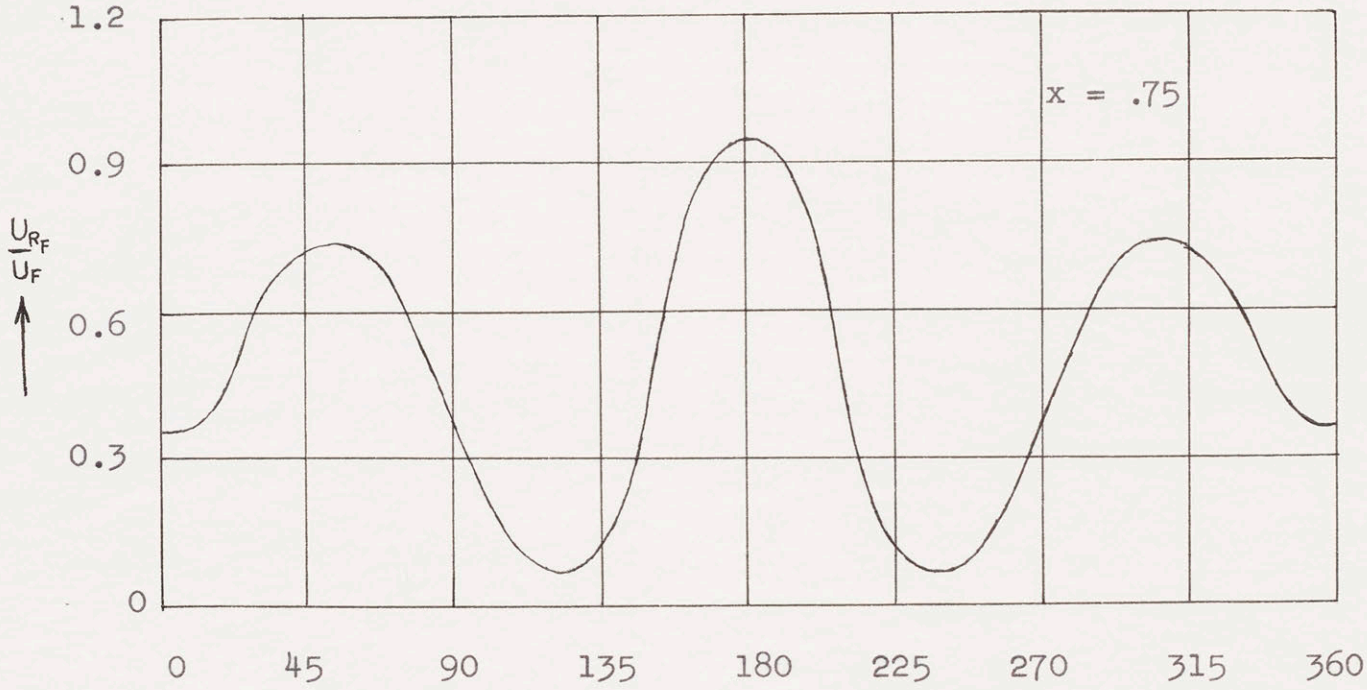

Fig. 23. Induced Velocity Ratio Versus Azimuth (1/R = .25, h/R = .25, μ = .10)

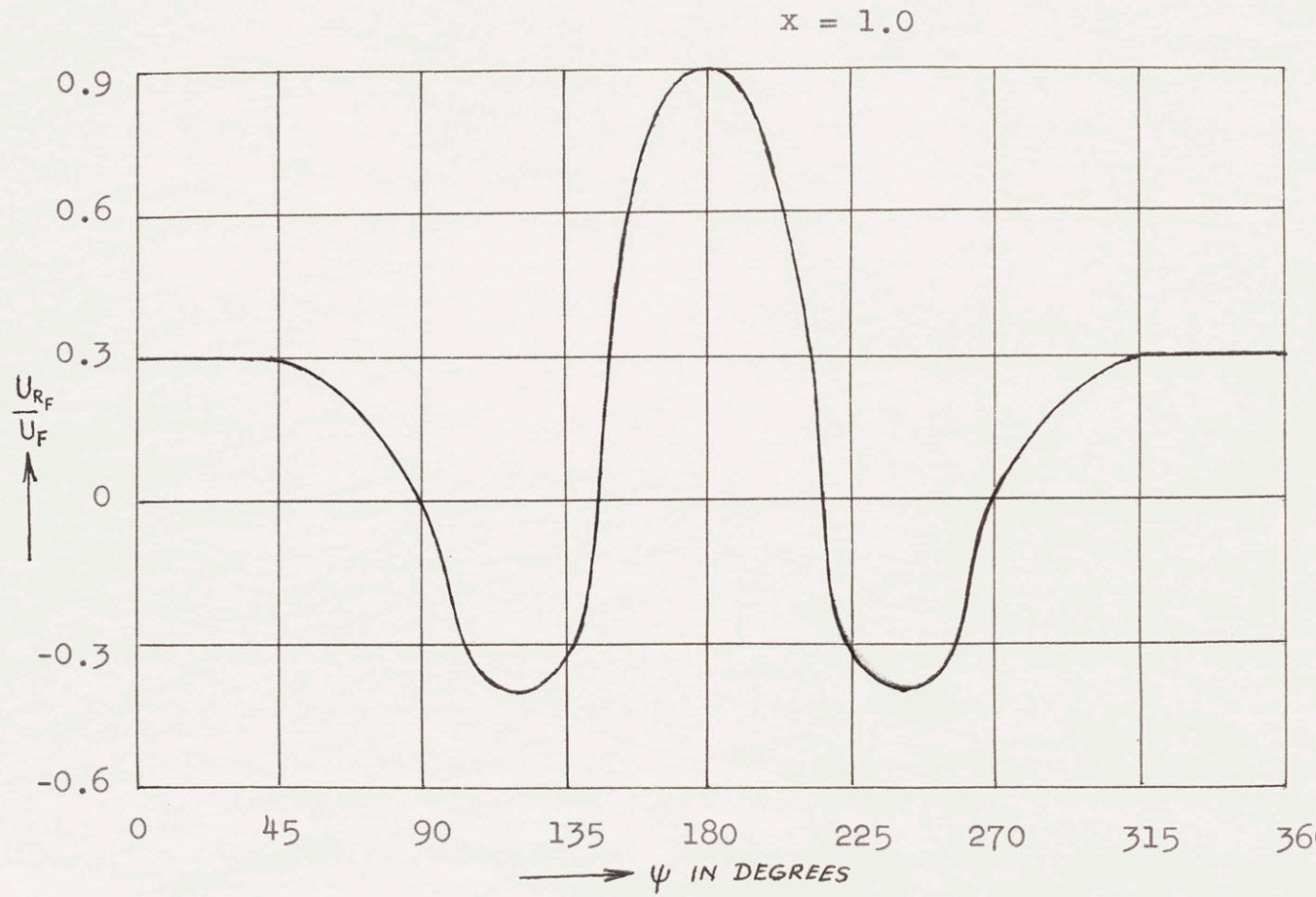

Fig. 24. Induced Velocity Ratio Versus Azimuth (1/R = .25, h/R = .25, μ = .10)

TABLE 1

Rotor and Blade Characteristics

Blade Radius (R)	4 ft.
Number of Blades (b)	3
Blade Chord (c)	5 in.
Airfoil Section	NACA 0012
Lift Curve Slope (a)	5.67 rad.
Rotor Solidity (σ)	0.0995
Lock Number (γ)	4.2
Running Mass (m)	0.015 slugs/ft

TABLE 2

Rear Rotor Calculated Thrust with Typical Disc Loading

$\alpha_R = 5^\circ$ $\theta_R = 10^\circ$ $\alpha_F = 10^\circ$ $\theta_F = 10^\circ$

$l/R = 0$ $h/R = .25$

N = 400 rpm

μ	.05	.10	.15	.20	.25
γ_{F_h}	.068	.058	.054	.056	.059
β_{1c}	-.0164	-.035	-.054	-.072	-.09
γ_{F_t}	.0672	.0545	.046	.042	.0365
χ	36.9°	61.5°	72.9°	78.2°	81.7°
$\bar{K}$	.10	.45	.70	.85	1.0
γ'_{R_h}	.068	.064	.06	.056	.055
T*	23.0	25.6	28.5	31.8	34.5
T**	27.3	30.8	35.0	38.0	40.5

* With Interference

** Without Interference

TABLE 3

Rear Rotor Calculated Thrust with Typical Disc Loading

$\alpha_R = 5^\circ$ $\theta_R = 10^\circ$ $\alpha_F = 10^\circ$ $\theta_F = 10^\circ$

$l/R = .25$ $h/R = .25$

N = 400 rpm

μ	.05	.10	.15	.20	.25
λ_{F_h}	.068	.058	.054	.056	.059
β_{1c}	-.0164	-.035	-.054	-.072	-.09
λ_{F_t}	.0672	.0545	.046	.042	.0365
χ	36.9°	61.5°	72.9°	78.2°	81.7°
$\bar{K}$	.15	.60	.80	.85	1.0
λ_{R_h}	.071	.0676	.0617	.056	.055
T*	21.6	23.9	27.6	31.8	34.5
T**	27.3	30.8	35.0	38.0	40.5

* With Interference

** Without Interference

TABLE 4

Rear Rotor Calculated Thrust with Typical Disc Loading

$\alpha_R = 5^\circ$ $\theta_R = 10^\circ$ $\alpha_F = 10^\circ$ $\theta_F = 10^\circ$

$l/R = .50$ $h/R = .25$

N = 400 rpm

μ	.05	.10	.15	.20	.25
λ_{F_h}	.068	.058	.054	.056	.059
β_{1c}	-.0164	-.035	-.054	-.072	-.09
λ_{F_t}	.0672	.0545	.046	.042	.0365
X	36.9°	61.5°	72.9°	78.2°	81.7°
$\overline{K}$	.25	.70	.88	1.0	1.0
λ'_{R_h}	.069	.07	.0633	.0585	.055
T*	22.5	22.8	27.0	30.6	34.5
T**	27.3	30.8	35.0	38.0	40.5

* With Interference

** Without Interference

TABLE 5

Rear Rotor Calculated Thrust with Uniform Disc Loading

$\alpha_R = 5^\circ$ $\theta_R = 10^\circ$ $\alpha_F = 10^\circ$ $\theta_F = 10^\circ$

$l/R = 0$ $h/R = .25$

N = 400 rpm

μ	.05	.10	.15	.20	.25
λ_{F_n}	.068	.058	.054	.056	.059
β_{1c}	-.0164	-.035	-.054	-.072	-.09
λ_{F_t}	.0672	.0545	.046	.042	.0365
X	36.9	61.5	72.9	78.2	81.7
$\bar{K}$	.10	.45	.70	.90	1.1
λ'_{R_n}	.068	.064	.06	.057	.0562
T*	23.0	25.6	28.5	31.4	34.0
T**	27.3	30.8	35.0	38.0	40.5

* With Interference

** Without Interference

TABLE 6

Rear Rotor Calculated Thrust with Uniform Disc Loading

$\alpha_R = 5^\circ$ $\theta_R = 10^\circ$ $\alpha_F = 10^\circ$ $\theta_F = 10^\circ$

$l/R = .25$ $h/R = .25$

N = 400 rpm

μ	.05	.10	.15	.20	.25
λ_{F_h}	.068	.058	.054	.056	.059
β_{IC}	-.0164	-.035	-.054	-.072	-.09
λ_{F_t}	.0672	.0545	.046	.042	.0365
X	36.9°	61.5°	72.9°	78.2°	81.7°
$\bar{K}$	.20	.60	.90	1.1	1.3
λ'_{R_h}	.071	.0676	.0636	.06	.0588
T*	21.6	23.9	26.7	30.0	32.7
T**	27.3	30.8	35.0	38.0	40.5

* With Interference

** Without Interference

TABLE 7

Rear Rotor Calculated Thrust with Uniform Disc Loading

$\alpha_R = 5^\circ$ $\theta_R = 10^\circ$ $\alpha_F = 10^\circ$ $\theta_F = 10^\circ$

$l/R = .50$ $h/R = .25$

N = 400 rpm

μ	.05	.10	.15	.20	.25
λ_{F_h}	.068	.058	.054	.056	.059
β_{IC}	-.0164	-.035	-.054	-.072	-.09
λ_{F_t}	.0672	.0545	.046	.042	.0365
X	36.9°	61.5°	72.9°	78.2°	81.7°
$\bar{K}$	.25	.70	1.0	1.2	1.45
λ'_{R_h}	.069	.07	.0656	.0617	.0607
T*	22.5	22.8	25.9	29.2	31.6
T**	27.3	30.8	35.0	38.0	40.5

* With Interference

** Without Interference

TABLE 8

Rear Rotor Calculated and Experimental Thrust for Various Overlap and Forward Speed

1/R	μ	Uniform Disc Loading	Typical Disc Loading	Experimental
	.05	23.0	23.0	22.5
	.10	25.6	25.6	24.8
0	.15	28.5	28.5	28.8
	.20	31.8	31.4	30.3
	.25	34.5	34.0	34.5
	.05	21.6	21.6	19.5
	.10	23.9	23.9	22.0
.25	.15	27.6	26.7	26.5
	.20	32.0	30.0	29.5
	.25	34.5	32.7	32.0
	.05	22.5	22.5	21.2
	.10	22.8	22.8	22.5
.50	.15	27.0	25.9	26.0
	.20	30.6	29.2	29.8
	.25	34.5	31.6	33.4

TABLE 9

Rear Rotor Calculated and Experimental Thrust, Without Interference Effect

$\alpha_R = 5^\circ$ $\theta_R = 10^\circ$ N = 400 rpm

μ	EXPERIMENTAL	THEORETICAL
.05	30.0	27.3
.10	33.5	30.8
.15	35.5	35.0
.20	38.3	38.0
.25	42.2	40.5

TABLE 10

Third Harmonic Cosine Inflow Coefficient -

Theoretical Values

ℓ/R	h/R	μ	λ_{3c}			
			x=.25	x=.50	x=.75	x=1.0
0	.25	.05	-.00212	-.00312	-.0072	-.0104
.25	.25	.05	-.00272	-.006	-.0092	-.0144
.25	.25	.10	-.0032	-.0075	-.012	-.012

NOTE: $\lambda_{3_s} \approx 0$

TABLE 11

Third Harmonic Vibratory Loads Due to Interference Effects - Theoretical and Experimental Results

$\alpha_R = 5^\circ$ $\theta_R = 0^\circ$ $\alpha_F = 10^\circ$ $\theta_F = 10^\circ$

N = 400 rpm h/R = .25

l/R	μ	Vibratory Loads (lbs)			
		Theoretical		Experimental	
		Cos 3ψ	Sin 3ψ	Cos 3ψ	Sin 3ψ
0	.05	-.23	-1.74	2.3	-2.3
.25	.05	-.36	-2.31	12.0	-1.1
.25	.10	-.4	-1.72	4.0	-1.8

REFERENCES

1. Heyson, Harry H. and Jewel, Joseph W., Charts of the Induced Velocities Near a Lifting Rotor, NASA Memorandum 4-15-59L, May 1959.

2. Duvivier, J.F., Study of Helicopter Rotor-Rotor Interference Effects on Hub Vibration, Technical Documentary Report No. ASD-TR-61-601, June 1962.

3. Mangler, K.W. and Squire, H.B., The Induced Velocity Field of a Rotor, R and M No. 2642, British A.R.C., May 1950.

4. Heyson, Harry H. and Katzoff, S., Induced Velocities Near a Lifting Rotor with Non-uniform Disc Loading, NACA Report No. 1319, 1957.

5. Gessow, Alfred and Myers, G.C., Aerodynamics of the Helicopter, The Macmillan Company, New York, 1952.

6. Castles, Walter, Jr., and De Leeuw, Jacob Henri, The Normal Component of the Induced Velocity in the Vicinity of a Lifting Rotor and Some Examples of its Application. NACA Report No. 1184, 1954.

7. Ham, Norman D. and Zvara, John, Experimental and Theoretical Analysis of Helicopter Rotor Hub Vibratory Forces. WADC Technical Report 59-522, October 1959.